

# Nucleon electromagnetic form factors on the lattice and in chiral effective field theory

M. Göckeler<sup>a,b</sup>, T.R. Hemmert<sup>c</sup>, R. Horsley<sup>d</sup>, D. Pleiter<sup>e</sup>,  
 P.E.L. Rakow<sup>f</sup>, A. Schäfer<sup>b</sup>, G. Schierholz<sup>e,g</sup>

QCDSF Collaboration

<sup>a</sup>*Institut für Theoretische Physik, Universität Leipzig, D-04109 Leipzig, Germany*

<sup>b</sup>*Institut für Theoretische Physik, Universität Regensburg, D-93040 Regensburg, Germany*

<sup>c</sup>*Physik-Department, Theoretische Physik, Technische Universität München, D-85747 Garching, Germany*

<sup>d</sup>*School of Physics, University of Edinburgh, Edinburgh EH9 3JZ, UK*

<sup>e</sup>*John von Neumann-Institut für Computing NIC, Deutsches Elektronen-Synchrotron DESY, D-15738 Zeuthen, Germany*

<sup>f</sup>*Theoretical Physics Division, Department of Mathematical Sciences, University of Liverpool, Liverpool L69 3BX, UK*

<sup>g</sup>*Deutsches Elektronen-Synchrotron DESY, D-22603 Hamburg, Germany*

---

## Abstract

We compute the electromagnetic form factors of the nucleon in quenched lattice QCD, using non-perturbatively improved Wilson fermions, and compare the results with phenomenology and chiral effective field theory.

*Key words:* Lattice QCD; effective field theory; chiral extrapolation; nucleon electromagnetic form factors

*PACS:* 11.15.Ha; 12.38.Gc; 13.40.Gp

---

## 1 Introduction

The measurements of the electromagnetic form factors of the proton and the neutron gave the first hints at an internal structure of the nucleon, and a theory

of the nucleon cannot be considered satisfactory if it is not able to reproduce the form factor data. For a long time, the overall trend of the experimental results for small and moderate values of the momentum transfer  $q^2$  could be described reasonably well by phenomenological (dipole) fits

$$\begin{aligned} G_e^p(q^2) &\sim \frac{G_m^p(q^2)}{\mu^p} \sim \frac{G_m^n(q^2)}{\mu^n} \\ &\sim \left(1 - q^2/m_D^2\right)^{-2}, \\ G_e^n(q^2) &\sim 0 \end{aligned} \tag{1.1}$$

with  $m_D \sim 0.84 \text{ GeV}$  and the magnetic moments

$$\mu^p \sim 2.79 \quad , \quad \mu^n \sim -1.91 \tag{1.2}$$

in units of nuclear magnetons. Recently, the form factors of the nucleon have been studied experimentally with high precision and deviations from this uniform dipole form have been observed, both at very small  $q^2$  [1] and in the region above  $1 \text{ GeV}^2$  [2,3].

It is therefore of great interest to derive the nucleon form factors from QCD. Since form factors are typical low-energy quantities, perturbation theory in terms of quarks and gluons is useless for this purpose and a non-perturbative method is needed. If one wants to avoid additional assumptions or models, one is essentially restricted to lattice QCD and Monte Carlo simulations. In view of the importance of nucleon form factors and the amount of experimental data available, it is surprising that there are only a few lattice investigations of form factors in the last years [4,5].

In this paper we give a detailed account of our results for the nucleon form factors obtained in quenched Monte Carlo simulations with non-perturbatively  $O(a)$ -improved Wilson fermions. We shall pay particular attention to the chiral extrapolation and compare with formulae from chiral effective field theory previously used for studies of the magnetic moments. The plan of the paper is as follows. After a few general definitions and remarks in the next section we describe the lattice technology that we used in Section 3. After commenting on our earlier attempts to perform a chiral extrapolation in Section 4, we investigate the quark-mass dependence of the form factors in more detail on a phenomenological basis in Section 5. We find that our data compare favourably with the recently observed deviations [2,3] from the uniform dipole parametrisation of the proton form factors. In Section 6 we collect and discuss formulae from chiral effective field theory, which are confronted with our Monte Carlo results in Section 7. Our conclusions are presented in Section 8. The Appendices contain tables of the form factors and of the corresponding dipole fits.

## 2 Generalities

Experimentally, the nucleon form factors are measured via electron scattering. Because the fine structure constant is so small, it is justified to describe this process in terms of one-photon exchange. So the scattering amplitude is given by

$$T_{fi} = e^2 \bar{u}_e(k'_e, s'_e) \gamma_\mu u_e(k_e, s_e) \frac{1}{q^2} \langle p', s' | J^\mu | p, s \rangle \quad (2.1)$$

with the electromagnetic current

$$J^\mu = \frac{2}{3} \bar{u} \gamma^\mu u - \frac{1}{3} \bar{d} \gamma^\mu d + \dots \quad (2.2)$$

Here  $p, p'$  are the nucleon momenta,  $k_e, k'_e$  are the electron momenta, and  $s, s', \dots$  are the corresponding spin vectors. The momentum transfer is defined as  $q = p' - p$ . With the help of the form factors  $F_1(q^2)$  and  $F_2(q^2)$  the nucleon matrix element can be decomposed as

$$\langle p', s' | J^\mu | p, s \rangle = \bar{u}(p', s') \left[ \gamma_\mu F_1(q^2) + i \sigma^{\mu\nu} \frac{q_\nu}{2M_N} F_2(q^2) \right] u(p, s) \quad (2.3)$$

where  $M_N$  is the mass of the nucleon. From the kinematics of the scattering process, it can easily be seen that  $q^2 < 0$ . In the following, we shall often use the new variable  $Q^2 = -q^2$ . We have  $F_1(0) = 1$  (in the proton) as  $J$  is a conserved current, while  $F_2(0)$  measures the anomalous magnetic moment in nuclear magnetons. For a classical point particle, both form factors are independent of  $q^2$ , so deviations from this behaviour tell us something about the extended nature of the nucleon. In electron scattering,  $F_1$  and  $F_2$  are usually re-written in terms of the electric and magnetic Sachs form factors

$$\begin{aligned} G_e(q^2) &= F_1(q^2) + \frac{q^2}{(2M_N)^2} F_2(q^2), \\ G_m(q^2) &= F_1(q^2) + F_2(q^2), \end{aligned} \quad (2.4)$$

as then the (unpolarised) cross section becomes a linear combination of squares of the form factors.

Throughout the whole paper we assume flavour SU(2) symmetry. Hence we can decompose the form factors into isovector and isoscalar components. In terms of the proton and neutron form factors the isovector form factors are given by

$$G_e^v(q^2) = G_e^p(q^2) - G_e^n(q^2), \quad G_m^v(q^2) = G_m^p(q^2) - G_m^n(q^2) \quad (2.5)$$

such that

$$G_m^v(0) = G_m^p(0) - G_m^n(0) = \mu^p - \mu^n = \mu^v = 1 + \kappa_v \quad (2.6)$$

with  $\mu^v$  ( $\kappa_v$ ) being the isovector (anomalous) magnetic moment  $\sim 4.71$  (3.71). In the actual simulations we do not work directly with these definitions when we calculate the isovector form factors. Instead we use the relation

$$\begin{aligned} & \langle \text{proton} | \left( \frac{2}{3} \bar{u} \gamma^\mu u - \frac{1}{3} \bar{d} \gamma^\mu d \right) | \text{proton} \rangle \\ & - \langle \text{neutron} | \left( \frac{2}{3} \bar{u} \gamma^\mu u - \frac{1}{3} \bar{d} \gamma^\mu d \right) | \text{neutron} \rangle \\ & = \langle \text{proton} | \left( \bar{u} \gamma^\mu u - \bar{d} \gamma^\mu d \right) | \text{proton} \rangle \end{aligned} \quad (2.7)$$

and compute the isovector form factors from proton matrix elements of the current  $\bar{u} \gamma^\mu u - \bar{d} \gamma^\mu d$ . Similarly one could use the isoscalar current  $\bar{u} \gamma^\mu u + \bar{d} \gamma^\mu d$  for the computation of isoscalar form factors.

### 3 Lattice technology

Using the standard Wilson gauge field action we have performed quenched simulations with  $O(a)$ -improved Wilson fermions (clover fermions). For the coefficient  $c_{SW}$  of the Sheikholeslami-Wohlert clover term we chose a non-perturbatively determined value calculated from the interpolation formula given in Ref. [6]. The couplings  $\beta = 6/g^2$  and  $c_{SW}$ , the lattice sizes and statistics, the values of the hopping parameter  $\kappa$  (not to be confused with an anomalous magnetic moment) and the corresponding pion and nucleon masses (in lattice units) are collected in Table 1. There we also give the nucleon masses extrapolated to the critical hopping parameter  $\kappa_c$ . This extrapolation has been performed (on the basis of a larger set of nucleon masses) by means of the ansatz

$$(aM_N)^2 = (aM_N^0)^2 + b_2(am_\pi)^2 + b_3(am_\pi)^3, \quad (3.1)$$

which provides a very good (phenomenological) description of the data [7]. Here  $M_N^0$  denotes the nucleon mass in the chiral limit. At the present level of accuracy, the difference between  $M_N^0$  and the physical nucleon mass can be neglected. Whenever we give numbers in physical units the scale has been set by the chirally extrapolated nucleon masses from Table 1.

In Fig. 1 we plot  $M_N^2$  versus  $m_\pi^2$  using the masses from Table 1. The picture demonstrates that scaling violations in the masses are small.

In order to compute nucleon masses or matrix elements we need suitable interpolating fields. For a proton with spatial momentum  $\vec{p}$  the most obvious choice in terms of the quark fields  $u(x)$  and  $d(x)$  is

Table 1

Simulation parameters, numbers of gauge field configurations used (# configs.) and masses.

$\beta$	$c_{SW}$	$\kappa$	Volume	# configs.	$am_\pi$	$aM_N$
6.0	1.769	0.1320	$16^3 \times 32$	$O(450)$	0.5412(9)	0.9735(40)
6.0	1.769	0.1324	$16^3 \times 32$	$O(550)$	0.5042(7)	0.9353(25)
6.0	1.769	0.1333	$16^3 \times 32$	$O(550)$	0.4122(9)	0.8241(34)
6.0	1.769	0.1338	$16^3 \times 32$	$O(500)$	0.3549(12)	0.7400(85)
6.0	1.769	0.1342	$16^3 \times 32$	$O(700)$	0.3012(10)	0.7096(48)
6.0	1.769	$\kappa_c = 0.1353$				0.5119(67)
6.2	1.614	0.1333	$24^3 \times 48$	$O(300)$	0.4136(6)	0.7374(21)
6.2	1.614	0.1339	$24^3 \times 48$	$O(300)$	0.3565(8)	0.6655(28)
6.2	1.614	0.1344	$24^3 \times 48$	$O(300)$	0.3034(6)	0.5963(29)
6.2	1.614	0.1349	$24^3 \times 48$	$O(500)$	0.2431(7)	0.5241(39)
6.2	1.614	$\kappa_c = 0.1359$				0.3695(36)
6.4	1.526	0.1338	$32^3 \times 48$	$O(200)$	0.3213(8)	0.5718(28)
6.4	1.526	0.1342	$32^3 \times 48$	$O(100)$	0.2836(9)	0.5266(31)
6.4	1.526	0.1346	$32^3 \times 48$	$O(200)$	0.2402(8)	0.4680(37)
6.4	1.526	0.1350	$32^3 \times 48$	$O(300)$	0.1933(7)	0.4156(34)
6.4	1.526	0.1353	$32^3 \times 64$	$O(300)$	0.1507(8)	0.3580(47)
6.4	1.526	$\kappa_c = 0.1358$				0.2800(53)

$$\begin{aligned}
B_\alpha(t, \vec{p}) &= \sum_{x, x_4=t} e^{-i\vec{p}\cdot\vec{x}} \epsilon_{ijk} u_\alpha^i(x) u_\beta^j(x) (C\gamma_5)_{\beta\gamma} d_\gamma^k(x), \\
\bar{B}_\alpha(t, \vec{p}) &= \sum_{x, x_4=t} e^{i\vec{p}\cdot\vec{x}} \epsilon_{ijk} \bar{d}_\beta^i(x) (C\gamma_5)_{\beta\gamma} \bar{u}_\gamma^j(x) \bar{u}_\alpha^k(x)
\end{aligned} \tag{3.2}$$

with the charge conjugation matrix  $C$  ( $\alpha, \beta, \gamma$  are Dirac indices,  $i, j, k$  are colour indices). Note that we now switch from Minkowski space to Euclidean space.

In Eq. (3.2) all three quarks sit at the same point. Clearly, as protons are not point objects this is not the best thing to do, and with the above interpolating fields we run the risk that the amplitudes of one-proton states in correlation functions might be very small making the extraction of masses and matrix elements rather unreliable. Therefore we employ two types of improvement: First we smear the sources and the sinks for the quarks in their time slices, secondly we apply a “non-relativistic” projection.

Our smearing algorithm (Jacobi smearing) is described in Ref. [8]. The parameters  $N_{\text{smear}}, \kappa_{\text{smear}}$  used in the actual computations and the resulting smearing radii are given in Table 2. A typical rms nucleon radius is about 0.8 fm, our smearing radii are about half that size.

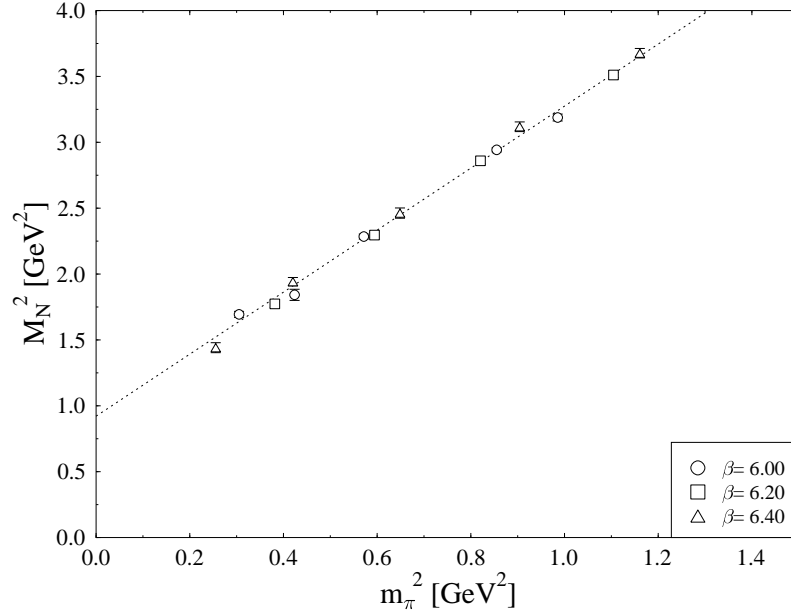


Fig. 1. Nucleon mass squared versus pion mass squared from the data in Table 1. The dotted straight line is just a guide to the eyes.

Table 2

Smearing parameters for Jacobi smearing.

$\beta$	$N_{\text{smear}}$	$\kappa_{\text{smear}}$	$r_{\text{rms}}$
6.0	50	0.21	$\sim 3.5a \sim 0.38 \text{ fm}$
6.2	100	0.21	$\sim 5.6a \sim 0.44 \text{ fm}$
6.4	150	0.21	$\sim 6.7a \sim 0.40 \text{ fm}$

The “non-relativistic” projection means that we replace each spinor by

$$\psi \rightarrow \psi^{NR} = \frac{1}{2}(1 + \gamma_4)\psi, \quad \bar{\psi} \rightarrow \bar{\psi}^{NR} = \bar{\psi}\frac{1}{2}(1 + \gamma_4). \quad (3.3)$$

This replacement leaves quantum numbers unchanged, but we would expect it to improve the overlap with baryons. Practically this means that for each baryon propagator we consider only the first two Dirac components. So we only have  $2 \times 3$  inversions to perform rather than the usual  $4 \times 3$  inversions – a saving of 50% in computer time.

The non-forward matrix elements required for the form factors are computed from ratios of three-point functions to two-point functions. The two-point

function is defined as

$$C_2(t, \vec{p}) = \sum_{\alpha\beta} \Gamma_{\beta\alpha} \langle B_\alpha(t, \vec{p}) \bar{B}_\beta(0, \vec{p}) \rangle \quad (3.4)$$

with the spin projection matrix

$$\Gamma = \frac{1}{2}(1 + \gamma_4) . \quad (3.5)$$

In the three-point function

$$C_3(t, \tau, \vec{p}, \vec{p}') = \sum_{\alpha\beta} \Gamma_{\beta\alpha} \langle B_\alpha(t, \vec{p}) \mathcal{O}(\tau) \bar{B}_\beta(0, \vec{p}') \rangle \quad (3.6)$$

we have used, besides the matrix (3.5) corresponding to unpolarised matrix elements, also

$$\Gamma = \frac{1}{2}(1 + \gamma_4) i\gamma_5 \gamma_2 \quad (3.7)$$

corresponding to polarisation in the 2-direction. We then computed the ratios

$$R(t, \tau, \vec{p}, \vec{p}') = \frac{C_3(t, \tau, \vec{p}, \vec{p}')}{C_2(t, \vec{p})} \times \left[ \frac{C_2(\tau, \vec{p}) C_2(t, \vec{p}) C_2(t - \tau, \vec{p}')}{C_2(\tau, \vec{p}') C_2(t, \vec{p}') C_2(t - \tau, \vec{p})} \right]^{1/2} . \quad (3.8)$$

If all time differences are sufficiently large, i.e. if  $0 \ll \tau \ll t$ ,  $R$  is proportional to the (polarised or unpolarised) proton matrix element of the operator  $\mathcal{O}$  with a known kinematical coefficient presented below.

For the electromagnetic form factors the operator to be studied is the vector current. In contrast to previous investigations [4,5], which used the conserved vector current, we chose to work with the local vector current  $\bar{\psi}(x) \gamma_\mu \psi(x)$ . The local vector current has to be renormalised, because it is not conserved. It should also be improved so that its matrix elements have discretisation errors of  $O(a^2)$  only, which means that we use the operator

$$V_\mu = Z_V (1 + b_V a m_q) \left[ \bar{\psi} \gamma_\mu \psi + \frac{1}{2} i c_V a \partial_\lambda (\bar{\psi} \sigma_{\mu\lambda} \psi) \right] , \quad (3.9)$$

where  $m_q$  is the bare quark mass:

$$a m_q = \frac{1}{2\kappa} - \frac{1}{2\kappa_c} . \quad (3.10)$$

We have taken  $Z_V$  and  $b_V$  from the parametrisations given by the ALPHA collaboration [9] (see also Ref. [10]). The improvement coefficient  $c_V$  has also been computed non-perturbatively [11]. The results can be represented by the expression [7]

$$c_V = -0.01225 \frac{4}{3} g^2 \frac{1 - 0.3113 g^2}{1 - 0.9660 g^2} , \quad (3.11)$$

from which we have calculated  $c_V$ . In the limit  $g^2 \rightarrow 0$  it agrees with perturbation theory [12]. Computing all these additional contributions in our simulations, we found the improvement terms to be numerically small. Note that the improvement coefficient  $c_{CVC}$  for the conserved vector current is only known to tree level so that a fully non-perturbative analysis would not be possible had we used the conserved vector current.

In order to describe the relation between the ratios we computed and the form factors let us call the ratio  $R$  for the  $\mu$ -component of the renormalised vector current more precisely  $R_\mu$ . Furthermore we distinguish the unpolarised case (spin projection matrix (3.5)) from the polarised case (spin projection matrix (3.7)) by a superscript. The (Minkowski) momentum transfer is given by

$$q^2 = -Q^2 = 2 \left( M_N^2 + \vec{p} \cdot \vec{p}' - E_N(\vec{p}) E_N(\vec{p}') \right) \quad (3.12)$$

with the nucleon energy

$$E_N(\vec{p}) = \sqrt{M_N^2 + \vec{p}^2}. \quad (3.13)$$

Using the abbreviation

$$A(\vec{p}, \vec{p}')^{-1} = (-Q^2 - 4M_N^2) \sqrt{E_N(\vec{p})(M_N + E_N(\vec{p})) E_N(\vec{p}')(M_N + E_N(\vec{p}'))} \quad (3.14)$$

we have

$$\begin{aligned} R_4^{\text{unpol}}(t, \tau, \vec{p}, \vec{p}') &= A(\vec{p}, \vec{p}') \left[ G_e(Q^2) M_N (E_N(\vec{p}) + E_N(\vec{p}')) \right. \\ &\quad \times \left( \vec{p}' \cdot \vec{p} - (M_N + E_N(\vec{p}))(M_N + E_N(\vec{p}')) \right) \\ &\quad \left. + G_m(Q^2) \left( (\vec{p}' \cdot \vec{p})^2 - \vec{p}^2 \vec{p}'^2 \right) \right], \end{aligned} \quad (3.15)$$

$$\begin{aligned} R_4^{\text{pol}}(t, \tau, \vec{p}, \vec{p}') &= A(\vec{p}, \vec{p}') i(p'_1 p_3 - p'_3 p_1) \left[ G_e(Q^2) M_N (E_N(\vec{p}) + E_N(\vec{p}')) \right. \\ &\quad \left. + G_m(Q^2) \left( \vec{p}' \cdot \vec{p} - (M_N + E_N(\vec{p}))(M_N + E_N(\vec{p}')) \right) \right], \end{aligned} \quad (3.16)$$

and for  $j = 1, 2, 3$

$$\begin{aligned} R_j^{\text{unpol}}(t, \tau, \vec{p}, \vec{p}') &= A(\vec{p}, \vec{p}') i \left[ G_e(Q^2) M_N (p_j + p'_j) \right. \\ &\quad \times \left( (M_N + E_N(\vec{p}))(M_N + E_N(\vec{p}')) - \vec{p}' \cdot \vec{p} \right) \\ &\quad + G_m(Q^2) \left( p_j (E_N(\vec{p}) \vec{p}'^2 - E_N(\vec{p}') \vec{p}' \cdot \vec{p}) \right. \\ &\quad \left. \left. + p'_j (E_N(\vec{p}') \vec{p}^2 - E_N(\vec{p}) \vec{p}' \cdot \vec{p}) \right) \right], \end{aligned} \quad (3.17)$$



$$\begin{aligned}
R_j^{\text{pol}}(t, \tau, \vec{p}, \vec{p}') &= A(\vec{p}, \vec{p}') \left[ G_e(Q^2) M_N(p_j + p'_j) (p'_1 p_3 - p'_3 p_1) \right. \\
&\quad + G_m(Q^2) (M_N(p_2 + p'_2) (\vec{p}' \times \vec{p})_j \\
&\quad + ((M_N + E_N(\vec{p}))(M_N + E_N(\vec{p}')) - \vec{p}' \cdot \vec{p}) \\
&\quad \left. \times \sum_{k=1}^3 \epsilon_{j2k} (p'_k E_N(\vec{p}) - p_k E_N(\vec{p}')) \right]. \tag{3.18}
\end{aligned}$$

Analogous expressions for the computation of the form factors  $F_1$  and  $F_2$  are obtained by inserting the definitions (2.4) in the above equations.

We have computed the ratios  $R$  in (3.8) (and the corresponding jackknife errors) for two choices of the momentum  $\vec{p}$ ,

$$\frac{L}{2\pi} \vec{p} = \begin{pmatrix} 0 \\ 0 \\ 0 \end{pmatrix}, \begin{pmatrix} 1 \\ 0 \\ 0 \end{pmatrix}, \tag{3.19}$$

and eight choices of the vector  $\vec{q} = \vec{p}' - \vec{p}$ ,

$$\begin{aligned}
\frac{L}{2\pi} \vec{q} = & \begin{pmatrix} 0 \\ 0 \\ 0 \end{pmatrix}, \begin{pmatrix} 0 \\ -1 \\ 0 \end{pmatrix}, \begin{pmatrix} 0 \\ -2 \\ 0 \end{pmatrix}, \begin{pmatrix} -1 \\ 0 \\ 0 \end{pmatrix}, \begin{pmatrix} -2 \\ 0 \\ 0 \end{pmatrix}, \\
& \begin{pmatrix} -1 \\ -1 \\ 0 \end{pmatrix}, \begin{pmatrix} -1 \\ -1 \\ -1 \end{pmatrix}, \begin{pmatrix} 0 \\ 0 \\ -1 \end{pmatrix}, \tag{3.20}
\end{aligned}$$

where  $L$  denotes the spatial extent of the lattice. Generically, several combinations of the above momenta lead to the same  $Q^2$ , and several ratios  $R$  contain the form factors at this  $Q^2$  with non-vanishing coefficients. Hence we determined  $G_e(Q^2)$  and  $G_m(Q^2)$  from a MINUIT fit of all these  $R$ s with the corresponding expressions (3.15) - (3.18) omitting all data points where the error for  $R$  was larger than 25%. The results are collected in the Tables in Appendix A. A missing entry indicates a case where the corresponding form factor could not be extracted, e.g. because we did not have sufficiently many  $R$ s with less than 25% error.

The nucleon masses used can be found in Table 1. The corresponding errors were, however, not taken into account when computing the errors of the form factors. Varying the nucleon masses within one standard deviation changed the form factors only by fractions of the quoted statistical error.

In general, the nucleon three-point functions consist of a quark-line connected contribution and a quark-line disconnected piece. Unfortunately, the quark-line disconnected piece is very hard to compute (for some recent attempts see

Refs. [13,14,15]). Therefore it is usually neglected, leading to one more source of systematic uncertainty. However, in the case of exact isospin invariance the disconnected contribution drops out in non-singlet quantities like the isovector form factors. That is why the isovector form factors (Tables 7 - 9) are our favourite observables. Nevertheless, we have also computed the proton form factors separately ignoring the disconnected contributions. The results are given in Tables 10 - 12. Regrettably, meaningful values of the electric form factor of the neutron could not be extracted from our data. The results for the neutron magnetic form factor are collected in Tables 13 - 15. Note that the isovector form factors have been computed directly (cf. Eq. (2.7)) and not as the difference of the proton and neutron form factors.

## 4 Chiral extrapolation: a first attempt

The quark masses in our simulations are considerably larger than in reality leading to pion masses above 500 MeV. Hence we cannot compare our results with experimental data without performing a chiral extrapolation. In a first analysis of the proton results (see Refs. [16,17]) we assumed a linear quark-mass dependence of the form factors. More precisely, we proceeded as follows.

Schematically, the relation between a ratio  $R$  (three-point function/two-point function) and the form factors  $G_e$ ,  $G_m$  can be written in the form

$$R = \langle p' | J | p \rangle + \dots = c_e G_e + c_m G_m \quad (4.1)$$

with known coefficients  $c_e$ ,  $c_m$  for each data point characterised by the momenta, the quark mass, the spin projection and the space-time component of the current. Assuming a linear quark-mass dependence of  $G_e$  and  $G_m$  we performed a 4-parameter fit,

$$R = c_e a_e(am_q) + c_e b_e + c_m a_m(am_q) + c_m b_m, \quad (4.2)$$

of all ratios  $R$  belonging to the same value of  $Q^2$  in the chiral limit. The resulting form factors in the chiral limit are typically larger than the experimental data. They can be fitted with a dipole form, but the masses from these fits are considerably larger than their phenomenological counterparts [16,17].

What could be the reason for this discrepancy? Several possibilities suggest themselves: finite-size effects, quenching errors, cut-off effects or uncertainties in the chiral extrapolation. The length  $L$  of the spatial boxes in our simulations is such that the inequality  $m_\pi L > 4$  holds in all cases. Previous experience suggests that in the quenched approximation this is sufficient to exclude considerable distortions of the results due to the finite volume. This assumption

is confirmed by simulations with Wilson fermions, where we have data on different volumes. Quenching errors are much more difficult to control. However, first simulations with dynamical fermions indicate that – for the rather heavy quarks we can deal with – the form factors do not change very much upon unquenching [17]. Having Monte Carlo data for three different lattice spacings (see Table 1) we can test for cut-off effects in the chirally extrapolated form factors, but we find them to be hardly significant. So our chiral extrapolation ought to be reconsidered. Indeed, the chiral extrapolation of lattice data has been discussed intensively in the recent literature (for the magnetic moments see, e.g., Refs. [18,19,20], for the electric charge radius of the proton see Ref. [21]), and it has been pointed out that the issue is highly non-trivial. Therefore we shall examine the quark-mass dependence of our form factors in more detail.

Ideally, one would like to identify a regime of parameters (quark masses in particular) where contact with chiral effective field theory (ChEFT) can be made on the basis of results like those presented for the nucleon form factors in Ref. [22]. Once the range of applicability of these low-energy effective field theories has been established, one can use them for a safe extrapolation to smaller masses. However, these schemes do not work for arbitrarily large quark masses (or pion masses), nor for arbitrarily large values of  $Q^2$ . In particular, the expressions for the form factors worked out in Ref. [22] can be trusted only up to  $Q^2 \approx 0.4 \text{ GeV}^2$  (see the discussion in Section 6.1 below). Unfortunately, from our lattice simulations we only have data for values of  $Q^2$  which barely touch the interval  $0 < Q^2 < 0.4 \text{ GeV}^2$ . Therefore we shall try to describe the  $Q^2$  dependence of the lattice data for each quark mass by a suitable ansatz (of dipole type) and then study the mass dependence of the corresponding parameters. The fit ansatz will also serve as an extrapolation of the magnetic form factor down to  $Q^2 = 0$ . Since we cannot compute  $G_m(0)$  directly, such an extrapolation is required anyway to determine the magnetic moment. (For a different method, which does not require an extrapolation, see Ref. [5].) In Section 7 we shall come back to a comparison with ChEFT.

## 5 Investigating the quark-mass dependence

The analysis of our form factor data sketched in Section 4 yielded results in the chiral limit without much control over the approach to that limit. In this section we want to study the quark-mass dependence of the form factors more thoroughly. As already mentioned, to this end we have to make use of a suitable description of the  $Q^2$  dependence.

Motivated by the fact that the experimentally measured form factors at small values of  $Q^2$  can be described by a dipole form (cf. Eq. (1.1)) we fitted our

data with the ansatz

$$\begin{aligned} G_l(Q^2) &= \frac{A_l}{(1 + Q^2/M_l^2)^2} \quad , \quad l = e, m, \\ F_i(Q^2) &= \frac{A_i}{(1 + Q^2/M_i^2)^2} \quad , \quad i = 1, 2. \end{aligned} \quad (5.1)$$

In the case of the form factors  $G_e$  ( $F_1$ ) we fixed  $A_e = 1$  ( $A_1 = 1$ ). Note that we do not require the dipole masses in the two form factors to coincide. Thus our ansatz can accomodate deviations of the ratio  $G_m(0)G_e(Q^2)/G_m(Q^2)$  from unity as they have been observed in recent experiments [1,2,3].

Indeed, for all masses considered in our simulations the lattice data can be described rather well by a dipole ansatz. In Fig. 2 we show examples of our data (for  $m_\pi = 0.648$  GeV) together with the dipole fits. The fit results are collected in Table 16 for the isovector form factors, in Table 17 for the proton form factors and in Table 18 for the magnetic form factor of the neutron.

In Figs. 3, 4 we plot the isovector electric dipole mass  $M_e^v$ , the isovector magnetic dipole mass  $M_m^v$  and the isovector magnetic moment  $\mu^v$  versus  $m_\pi$ . We make the following observations.

Scaling violations in the dipole masses seem to be small, since the results do not show a definite trend as  $\beta$  grows from 6.0 to 6.4. For the magnetic moments the situation is less clear. There might be some systematic shift, though not much larger than the statistical errors.

The electric dipole masses tend to become slightly smaller than the magnetic dipole masses as the pion mass decreases though it is not clear whether this difference is statistically significant. This behaviour agrees qualitatively with the recent JLAB data [2,3] for  $G_e/G_m$  in the proton (see Fig. 5 below).

The data for the electric dipole masses suggest a linear dependence on  $m_\pi$ . Therefore we could not resist temptation to perform linear fits of the dipole masses and moments in Tables 16 - 18 in order to obtain values at the physical pion mass. Of course, at some point the singularities and non-analyticities arising from the Goldstone bosons of QCD must show up and will in some observables lead to a departure from the simple linear behaviour. It is however conceivable that this happens only at rather small pion masses (perhaps even only below the physical pion mass) and thus does not influence the value at the physical pion mass too strongly.

We performed the fits separately for each  $\beta$  value as well as for the combined data from all three  $\beta$  values. The results are presented in Table 3 together with the experimental numbers. For the isovector dipole masses and the isovector

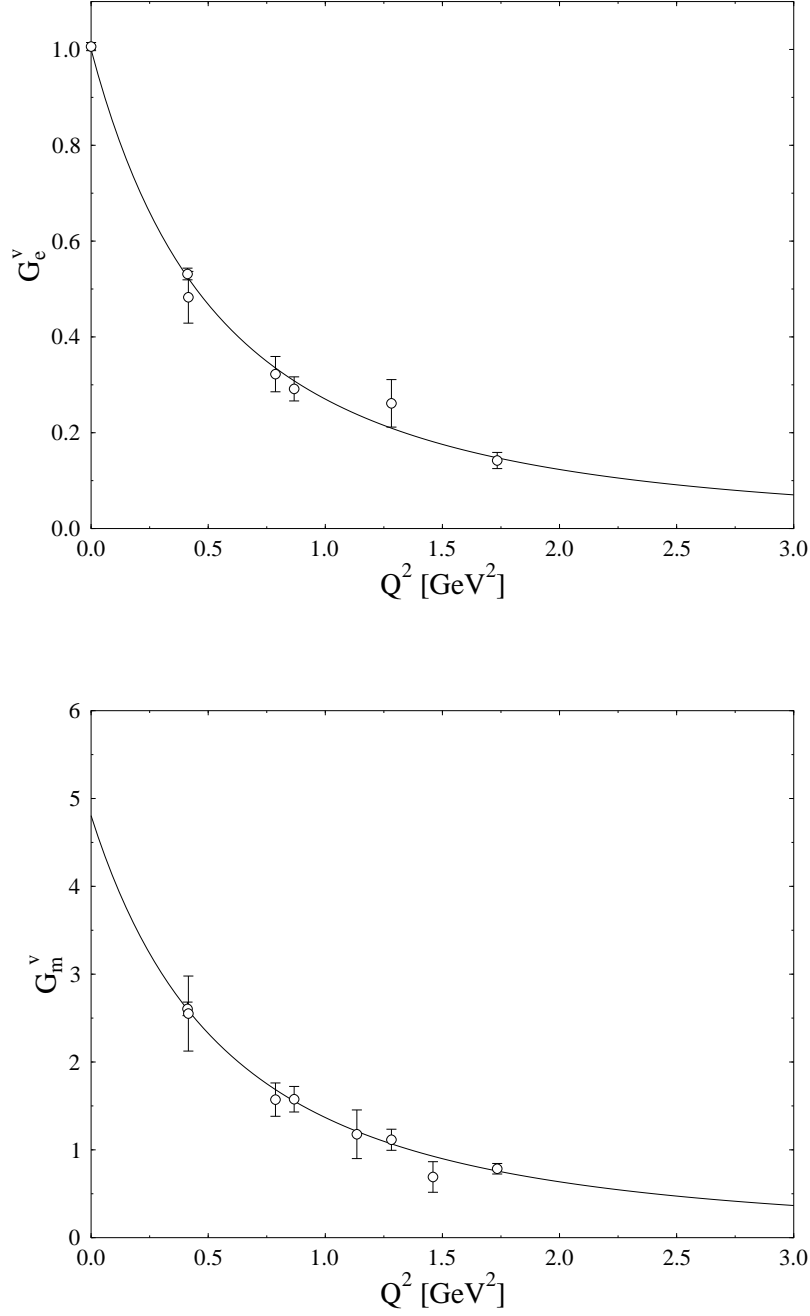


Fig. 2. Dipole fits of  $G_e^v$  data (top) and  $G_m^v$  data (bottom) at  $\beta = 6.4$  and  $m_\pi = 0.648 \text{ GeV}$ .

magnetic moment the fit curves (from the joint fits for all  $\beta$  values) are plotted in Figs. 3, 4. The corresponding plots for the proton and neutron data look similar. In the case of the electric dipole mass, the extrapolated result lies remarkably close to the experimental value. For the magnetic dipole mass and the magnetic moment the agreement is less good, but still satisfactory in view

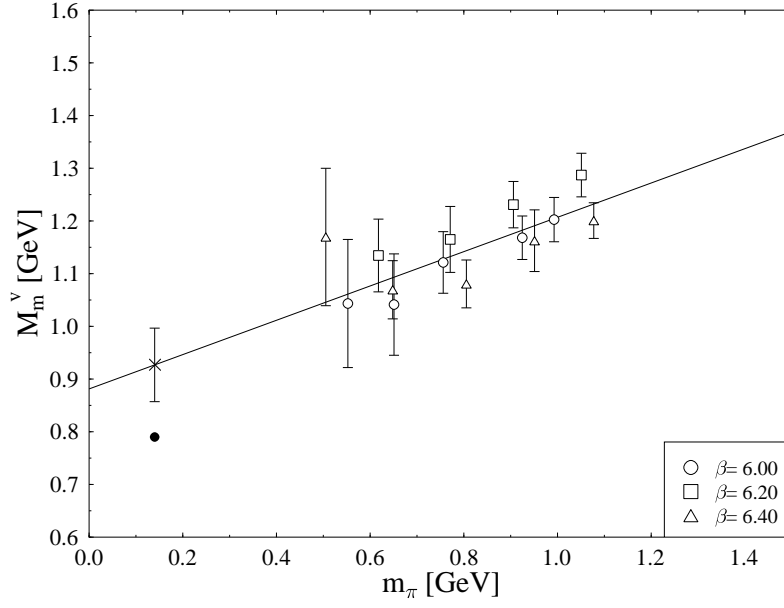
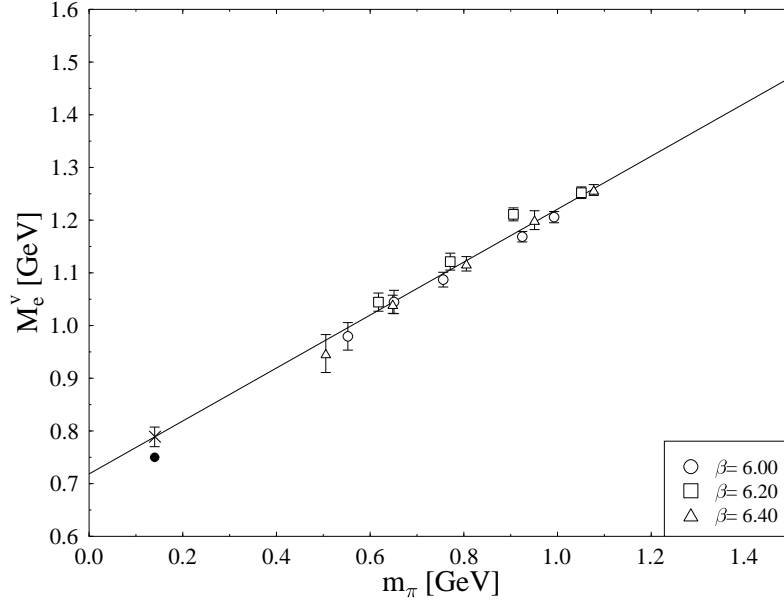


Fig. 3. Isovector dipole masses together with linear fits. The extrapolated value at the physical pion mass is marked by a cross. The solid circle indicates the phenomenological value computed from the radii given in Ref. [23].

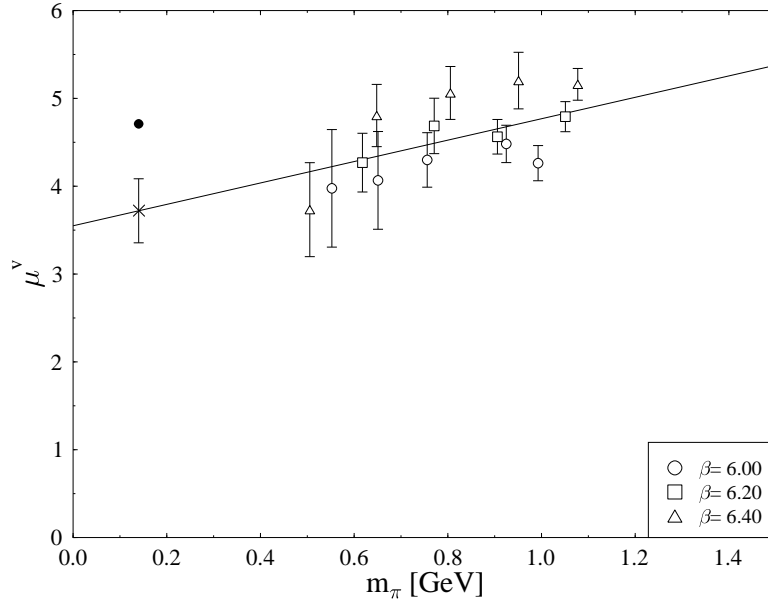


Fig. 4. Isovector magnetic moment together with a linear fit. The extrapolated value at the physical pion mass is marked by a cross. The solid circle indicates the experimental value.

Table 3

Results at the physical pion mass from linear fits, separately for each  $\beta$  value as well as for the combined data. The experimental numbers for  $M_e^v$  and  $M_m^v$  were derived from the radii given in Ref. [23] (cf. Eq. (6.11) below).

	$\beta = 6.0$	$\beta = 6.2$	$\beta = 6.4$	combined	experiment
$M_e^v$ [GeV]	0.78(3)	0.82(3)	0.77(3)	0.789(19)	0.75
$M_m^v$ [GeV]	0.87(15)	0.94(13)	0.93(10)	0.93(7)	0.79
$\mu^v$	3.9(8)	3.9(6)	3.9(6)	3.7(4)	4.71
$M_e^p$ [GeV]	0.80(3)	0.84(3)	0.80(2)	0.807(15)	0.84
$M_m^p$ [GeV]	0.93(15)	0.94(13)	0.92(10)	0.93(7)	0.84
$\mu^p$	2.3(5)	2.4(4)	2.4(3)	2.3(2)	2.79
$M_m^n$ [GeV]	0.83(16)	0.88(15)	0.91(11)	0.89(8)	0.84
$\mu^n$	-1.6(4)	-1.6(3)	-1.5(3)	-1.47(17)	-1.91

of the relatively large statistical errors.

Using the dipole approximations of the proton form factors with the extrapolated dipole masses as given in the fifth column of Table 3 we can now compare

$$\mu^p \frac{G_e^p(Q^2)}{G_m^p(Q^2)} = \frac{(1 + Q^2/(M_m^p)^2)^2}{(1 + Q^2/(M_e^p)^2)^2} \quad (5.2)$$

with the experimental data from Refs. [2,3]. This is done in Fig. 5. Especially for the larger values of  $Q^2$  we find good agreement, although the lattice data only cover the range  $Q^2 < 2 \text{ GeV}^2$  and for  $Q^2 > 2 \text{ GeV}^2$  the curve represents an extrapolation. It is perhaps not too surprising that the agreement improves as  $Q^2$  grows: Larger  $Q^2$  probe smaller distances inside the proton where the influence of the pion cloud, which is only insufficiently taken into account in the quenched approximation, is diminished.

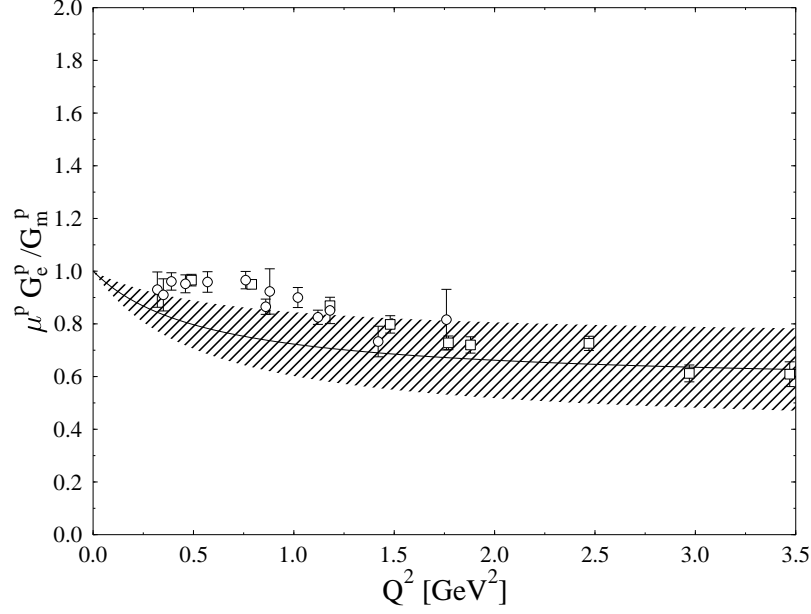


Fig. 5. The ratio  $\mu^p G_e^p / G_m^p$  from the chirally extrapolated dipole fits of the proton form factors (curve) compared with the experimental data from Refs. [2] (squares) and [3] (circles). The error band (indicated by the hatched area) has been computed from the errors of the extrapolated dipole masses. For the experimental numbers only the statistical errors are shown.

## 6 Results from chiral effective field theory

### 6.1 Form factors

For the comparison with ChEFT we choose the isovector form factors, because they do not suffer from the problem of quark-line disconnected contributions. Recently, a calculation for the quark-mass dependence of the isovector



anomalous magnetic moment has been presented [18]. The authors employed a ChEFT with explicit nucleon and  $\Delta$  degrees of freedom, called the Small Scale Expansion (SSE) [24]. It was argued [18] that the standard power-counting of ChEFT had to be changed to obtain a well-behaved chiral expansion – in particular, the leading isovector  $N\Delta$  transition coupling  $c_V$  (not to be confused with the improvement coefficient used earlier) had to be included in the leading-order Lagrangian. For details we refer to Ref. [18]. Here we extend this analysis from the magnetic moments to the Dirac and Pauli form factors of the nucleon, utilizing the same Lagrangians and couplings as in [18]. To leading one-loop order ( $\mathcal{O}(\epsilon^3)$  in SSE) 12 diagrams shown in Fig. 6 have to be evaluated in addition to the short-distance contributions. The calculation

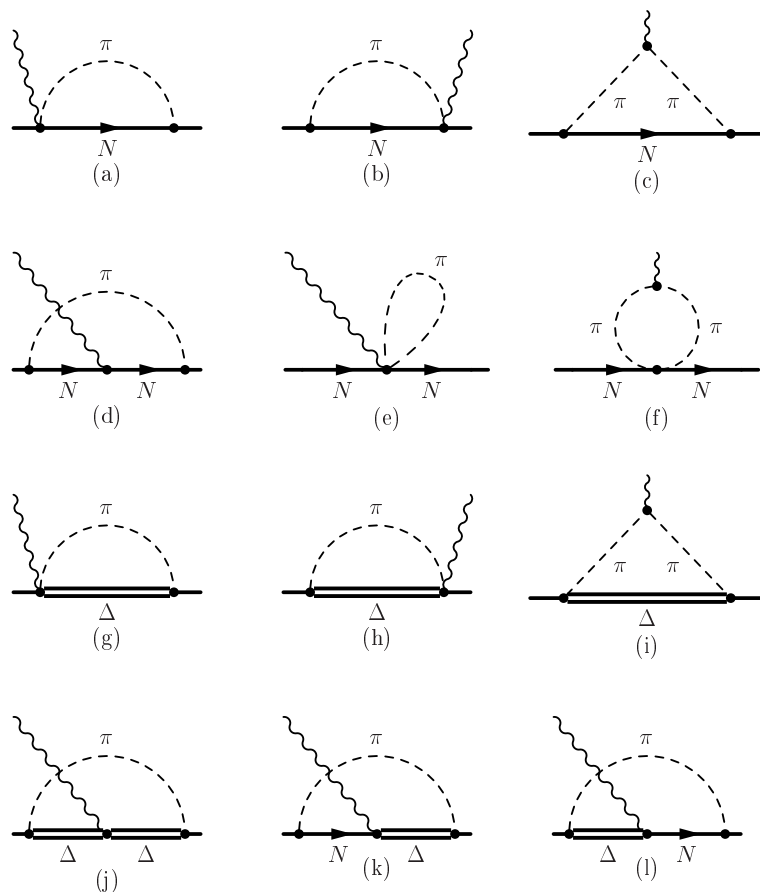


Fig. 6. One-loop diagrams in SSE contributing to the electromagnetic form factors. The wiggly line represents an external vector field.

follows very closely the one presented in Ref. [22], where further technical details of form factor calculations in ChEFT are discussed. The main difference between our analysis here and Ref. [22] arises from the modified counting of  $c_V$ , leading to the additional diagrams (k) and (l) in Fig. 6. Evaluating the diagrams in the Breit frame, we identify the isovector form factors  $F_1^v(q^2)$  and  $F_2^v(q^2)$  via the  $\mathcal{O}(\epsilon^3)$  relation for the proton matrix element

$$\begin{aligned}
& \langle p_2 | \left( \bar{u} \gamma_\mu u - \bar{d} \gamma_\mu d \right) | p_1 \rangle_{\text{Breit}} \\
&= \frac{e}{N_1 N_2} \bar{u}_v(r_2) \left[ \left( F_1^v(q^2) + \frac{q^2}{4(M_N^{\text{phys}})^2} F_2^v(0) + \mathcal{O}(\epsilon^4) \right) v_\mu \right. \\
&\quad \left. + \frac{1}{M_N^{\text{phys}}} \left( F_1^v(0) + F_2^v(q^2) + \mathcal{O}(\epsilon^4) \right) [S_\mu, S_\nu] q^\nu \right] u_v(r_1) \quad (6.1)
\end{aligned}$$

written in Minkowski space notation. Here  $M_N^{\text{phys}}$  is the physical nucleon mass and  $u_v(r_i)$  denotes a nucleon spinor with the normalisation

$$N_i = \sqrt{\frac{p_i^0 + M_N^{\text{phys}}}{2M_N^{\text{phys}}}} \quad , \quad i = 1, 2. \quad (6.2)$$

The quantity  $S_\mu$  denotes the Pauli-Lubanski spin-vector,  $S_\mu = \frac{i}{2} \gamma_5 \sigma_{\mu\nu} v^\nu$ . The four-vector  $v^\mu$  ( $v^2 = 1$ ) is connected to the usual four-momentum vector  $p^\mu = M_N^0 v^\mu + r^\mu$ , where  $M_N^0$  denotes the nucleon mass in the chiral limit and  $r_\mu$  is a soft momentum. Further details regarding calculations in this non-relativistic ChEFT can be found in Ref. [24].

We obtain

$$\begin{aligned}
F_1^v(q^2) = & 1 + \frac{1}{(4\pi F_\pi)^2} \left\{ q^2 \left( \frac{68}{81} c_A^2 - \frac{2}{3} g_A^2 - 2B_{10}^{(r)}(\lambda) \right) \right. \\
& + q^2 \left( \frac{40}{27} c_A^2 - \frac{5}{3} g_A^2 - \frac{1}{3} \right) \log \left[ \frac{m_\pi}{\lambda} \right] \\
& + \int_0^1 dx \left[ \frac{16}{3} \Delta^2 c_A^2 + m_\pi^2 \left( 3g_A^2 + 1 - \frac{8}{3} c_A^2 \right) \right. \\
& \left. - q^2 x(1-x) \left( 5g_A^2 + 1 - \frac{40}{9} c_A^2 \right) \right] \log \left[ \frac{\tilde{m}^2}{m_\pi^2} \right] \\
& + \int_0^1 dx \left[ \frac{32}{9} c_A^2 q^2 x(1-x) \frac{\Delta \log R(\tilde{m})}{\sqrt{\Delta^2 - \tilde{m}^2}} \right] \\
& \left. - \int_0^1 dx \frac{32}{3} c_A^2 \Delta \left[ \sqrt{\Delta^2 - m_\pi^2} \log R(m_\pi) - \sqrt{\Delta^2 - \tilde{m}^2} \log R(\tilde{m}) \right] \right\} \quad (6.3)
\end{aligned}$$

for the isovector Dirac form factor and

$$\begin{aligned}
F_2^v(q^2) = & \kappa_v(m_\pi) - g_A^2 \frac{4\pi M_N}{(4\pi F_\pi)^2} \int_0^1 dx \left[ \sqrt{\tilde{m}^2} - m_\pi \right] \\
& + \frac{32c_A^2 M_N \Delta}{9(4\pi F_\pi)^2} \int_0^1 dx \left[ \frac{1}{2} \log \left[ \frac{\tilde{m}^2}{4\Delta^2} \right] - \log \left[ \frac{m_\pi}{2\Delta} \right] \right. \\
& \left. + \frac{\sqrt{\Delta^2 - \tilde{m}^2}}{\Delta} \log R(\tilde{m}) - \frac{\sqrt{\Delta^2 - m_\pi^2}}{\Delta} \log R(m_\pi) \right] \quad (6.4)
\end{aligned}$$

for the isovector Pauli form factor, where we have used the abbreviations

$$R(m) = \frac{\Delta}{m} + \sqrt{\frac{\Delta^2}{m^2} - 1}, \quad \tilde{m}^2 = m_\pi^2 - q^2 x(1-x). \quad (6.5)$$

Furthermore, the isovector anomalous magnetic moment  $\kappa_v(m_\pi)$  appearing in Eq. (6.4) is given by

$$\begin{aligned} \kappa_v(m_\pi) = & \kappa_v^0 - \frac{g_A^2 m_\pi M_N}{4\pi F_\pi^2} \\ & + \frac{2c_A^2 \Delta M_N}{9\pi^2 F_\pi^2} \left\{ \sqrt{1 - \frac{m_\pi^2}{\Delta^2}} \log R(m_\pi) + \log \left[ \frac{m_\pi}{2\Delta} \right] \right\} \\ & - 8E_1^{(r)}(\lambda) M_N m_\pi^2 + \frac{4c_A c_V g_A M_N m_\pi^2}{9\pi^2 F_\pi^2} \log \left[ \frac{2\Delta}{\lambda} \right] + \frac{4c_A c_V g_A M_N m_\pi^3}{27\pi F_\pi^2 \Delta} \\ & - \frac{8c_A c_V g_A \Delta^2 M_N}{27\pi^2 F_\pi^2} \left\{ \left( 1 - \frac{m_\pi^2}{\Delta^2} \right)^{3/2} \log R(m_\pi) \right. \\ & \quad \left. + \left( 1 - \frac{3m_\pi^2}{2\Delta^2} \right) \log \left[ \frac{m_\pi}{2\Delta} \right] \right\}. \quad (6.6) \end{aligned}$$

Note that this expression corresponds to case *C* in the terminology of Ref. [18]. Of course, it agrees with the result obtained in Ref. [18] because  $\kappa_v(m_\pi)$  is automatically contained in a calculation of the form factors, as can be seen from the diagrams of Fig. 6.

The expressions (6.3) and (6.4) contain a number of phenomenological parameters: the pion decay constant  $F_\pi$ , the leading axial  $N\Delta$  coupling  $c_A$  (denoted by  $g_{\pi N\Delta}$  in Ref. [22]), the axial coupling of the nucleon  $g_A$ , the nucleon mass  $M_N$  and the  $\Delta(1232)$ -nucleon mass splitting  $\Delta = M_\Delta - M_N$ . In addition, there is one parameter not directly related to phenomenology,  $B_{10}^{(r)}(\lambda)$ . This counterterm at the renormalisation scale  $\lambda$  parametrises short-distance contributions to the Dirac radius discussed in the next subsection. Further parameters are encountered in the expression (6.6) for  $\kappa_v(m_\pi)$ : the isovector anomalous magnetic moment of the nucleon in the chiral limit  $\kappa_v^0$ , the leading isovector  $N\Delta$  coupling  $c_V$  and the counterterm  $E_1^{(r)}(\lambda)$ , which leads to quark-mass dependent short-distance contributions to  $\kappa_v$ .

The only difference of the above results for the form factors compared to the formulae given in Ref. [22] lies in the mass dependence of  $\kappa_v(m_\pi)$ , as the two additional diagrams (l) and (k) of Fig. 6 do not modify the momentum dependence. The authors of Ref. [22] were only interested in the physical point  $m_\pi = m_\pi^{\text{phys}}$ . Hence they fixed  $\kappa_v(m_\pi^{\text{phys}})$  to the empirical value  $\kappa_v^{\text{phys}} = 3.71$ . In addition, one may determine the counterterm  $B_{10}^{(r)}$  such that the phenomeno-

Table 4

Empirical values of the parameters.

Parameter	Empirical value
$g_A$	1.267
$c_A$	1.125
$F_\pi$	0.0924 GeV
$M_N$	0.9389 GeV
$\Delta$	0.2711 GeV
$\kappa_v^{\text{phys}}$	3.71
$\kappa_s^{\text{phys}}$	-0.12

logical value of the isovector Dirac radius  $r_1^v$  is reproduced. This leads to  $B_{10}^{(r)}(600 \text{ MeV}) = 0.34$ . Using for the other parameters the phenomenological values as given in Table 4 and inserting (6.3) and (6.4) in (2.4) one gets a rather good agreement with the experimental Sachs form factors for values of  $Q^2$  up to about  $0.4 \text{ GeV}^2$ , as exemplified in Fig. 7 by a comparison with the dispersion-theoretical description [23] of the isovector form factors. In addition we show in Fig. 7 the dipole approximations derived from the SSE formulae, which will be explained in Section 6.2.

Here we want to study the quark-mass dependence of the form factors. Strictly speaking, in such a study all the parameters should be taken in the chiral limit. To order  $\epsilon^3$  in the SSE, the  $m_\pi$  dependence of  $F_1$  and  $F_2$  is then given by the expressions (6.3), (6.4), (6.6). For comparison we note that in Ref. [22] a function  $\kappa_v(m_\pi)$  was found which corresponds to scheme  $B$  in the language of Ref. [18]. In this latter paper, scheme  $B$  was however shown to be insufficient to describe large-mass lattice data while scheme  $C$  turned out to work much better. Another recent calculation [25] of the nucleon form factors utilizes a relativistic framework for baryon chiral perturbation theory. However, as demonstrated in Ref. [18], it is not able to describe the mass dependence of the lattice data for  $\kappa_v$ . Therefore we shall not consider it for our fits.

Unfortunately, for most of the parameters the values in the chiral limit are only poorly known. That is why we shall usually work with the phenomenological numbers as given in Table 4 with the notable exception of the anomalous magnetic moment.

From our lattice simulations we only have data for values of  $Q^2$  which barely touch the interval  $0 < Q^2 < 0.4 \text{ GeV}^2$ . Therefore a direct comparison with (6.3) and (6.4) does not make sense (although the  $Q^2$  range in which the leading one-loop results of Eqs. (6.3) and (6.4) are applicable could depend on  $m_\pi$ ) and we have to resort to another procedure, which exploits the dipole

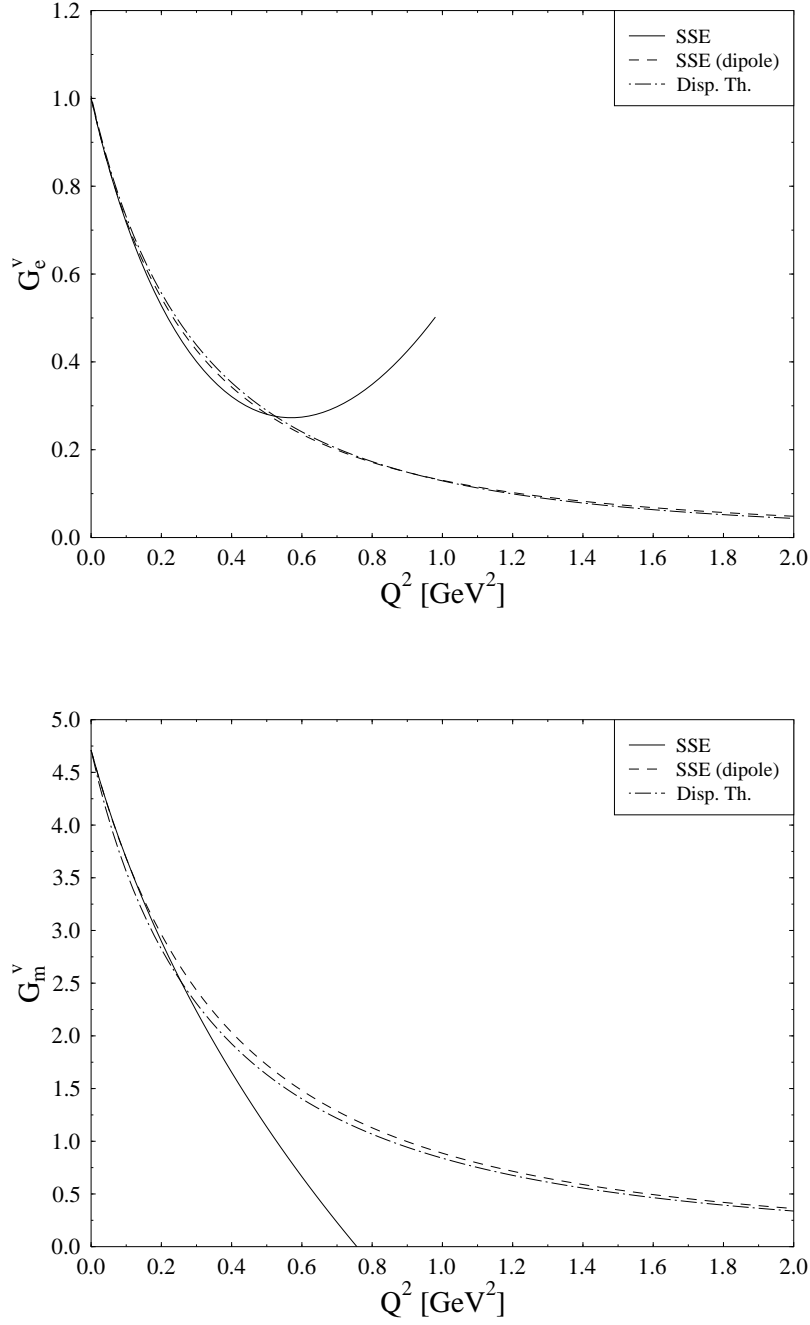


Fig. 7. Comparison of the dispersion-theoretical description of the isovector nucleon form factors with the SSE curves and the dipole approximations following from the SSE.

fits of our lattice form factors (see Section 7).

When one wants to apply (6.6) to lattice data obtained at unphysical pion masses  $m_\pi$  (and hence unphysical nucleon masses  $M_N$ ) one has to remember

that  $G_m(0) = 1 + \kappa$  is the magnetic moment in units of the nuclear magneton, i.e. the dimensionful magnetic moment is given by

$$(1 + \kappa) \frac{e}{2M_N}. \quad (6.7)$$

Here  $M_N$  is the nucleon mass as it is “measured” on the lattice for the quark mass considered, which is also used in the extraction of the form factors from the matrix elements (see Eqs. (2.3), (2.4)). On the other hand, Eq. (6.6) refers to the nuclear magneton calculated with the physical nucleon mass  $M_N^{\text{phys}}$ . Hence it is the “normalised”  $\kappa^{\text{norm}}$  obtained from

$$(1 + \kappa^{\text{norm}}) \frac{e}{2M_N^{\text{phys}}} = (1 + \kappa) \frac{e}{2M_N} \Rightarrow \kappa^{\text{norm}} = (1 + \kappa) \frac{M_N^{\text{phys}}}{M_N} - 1 \quad (6.8)$$

that should be compared (fitted) with (6.6).

## 6.2 Radii

The dipole masses of the form factors are closely related to the radii  $r_i$  defined by the Taylor expansion of  $F_i$  around  $q^2 = 0$ :

$$F_i(q^2) = F_i(0) \left[ 1 + \frac{1}{6} r_i^2 q^2 + \mathcal{O}(q^4) \right]. \quad (6.9)$$

If one describes the Sachs form factors by the dipole formulae

$$G_e(q^2) = \frac{1}{(1 + Q^2/M_e^2)^2}, \quad G_m(q^2) = \frac{G_m(0)}{(1 + Q^2/M_m^2)^2}, \quad (6.10)$$

the masses  $M_e$  and  $M_m$  are related to the above radii by

$$\frac{1}{M_e^2} = \frac{r_1^2}{12} + \frac{\kappa}{8M_N^2}, \quad \frac{1}{M_m^2} = \frac{r_1^2 + \kappa r_2^2}{12(1 + \kappa)}. \quad (6.11)$$

We note again that we do not demand the two dipole masses to be equal. Hence violations of the uniform dipole behaviour can be accounted for.

From Eqs. (6.3) and (6.4) we calculate the radii to  $\mathcal{O}(\epsilon^3)$  in SSE. For the isovector Dirac radius one obtains

$$\begin{aligned}
(r_1^v)^2 = & -\frac{1}{(4\pi F_\pi)^2} \left\{ 1 + 7g_A^2 + (10g_A^2 + 2) \log \left[ \frac{m_\pi}{\lambda} \right] \right\} - \frac{12B_{10}^{(r)}(\lambda)}{(4\pi F_\pi)^2} \\
& + \frac{c_A^2}{54\pi^2 F_\pi^2} \left\{ 26 + 30 \log \left[ \frac{m_\pi}{\lambda} \right] \right. \\
& \left. + 30 \frac{\Delta}{\sqrt{\Delta^2 - m_\pi^2}} \log \left[ \frac{\Delta}{m_\pi} + \sqrt{\frac{\Delta^2}{m_\pi^2} - 1} \right] \right\}. \tag{6.12}
\end{aligned}$$

The terms in the first bracket of Eq. (6.12) originate from Goldstone boson dynamics around a spin 1/2 nucleon (diagrams (a)-(f) in Fig. 6), the counter term  $B_{10}^{(r)}(\lambda)$ , which depends on the regularisation scale  $\lambda$ , parametrises short-distance contributions to the Dirac radius (“the nucleon core”) and the terms in the second bracket arise from Goldstone boson fluctuations around an intermediate  $\Delta(1232)$  state (diagrams (g)-(l) in Fig. 6). Evaluating these terms at an intermediate regularisation scale  $\lambda = 600$  MeV with the parameters given in Table 4 one obtains

$$(r_1^v)^2 = (0.41 (N\pi) + 0.29 (\Delta\pi)) \text{ fm}^2 - \frac{12 B_{10}^{(r)}(600 \text{ MeV})}{(4\pi F_\pi)^2}. \tag{6.13}$$

Note that the total result for  $(r_1^v)^2$  depends only rather weakly on the regularisation scale when  $\lambda$  varies between 500 and 700 MeV, as the scale dependence of the  $N\pi$  and the  $\Delta\pi$  contributions works in opposite direction.

Compared to the empirical value  $(r_1^v)_{\text{exp}}^2 = 0.585 \text{ fm}^2$  [23] the leading one-loop contributions from the Goldstone boson cloud tend to overestimate the Dirac radius (squared) by 20%. In Ref. [22] it was argued that one can always adjust the short-distance counter term  $B_{10}^{(r)}(\lambda)$  to reproduce the physical isovector Dirac radius, e.g.,  $B_{10}^{(r)}(600 \text{ MeV}) = 0.34$  works for the parameters of Table 4.

Here, however, we do not want to follow this philosophy. It would mean that the leading contribution of the “nucleon core” to the square of the isovector Dirac radius becomes *negative*. We consider such a scenario as unphysical. In the following we therefore set  $B_{10}^{(r)}(600 \text{ MeV}) = 0$  (vanishing core contribution) and conclude that the  $\mathcal{O}(\epsilon^3)$  SSE formula of Eq. (6.12) is not accurate enough to describe the quark-mass dependence of the isovector Dirac radius. Hence we can only expect a qualitative picture of the chiral extrapolation curve for this quantity, as shown in Section 7.2.

For the leading one-loop isovector Pauli radius (squared) one obtains

$$\begin{aligned}
(r_2^v)^2 = & \frac{g_A^2 M_N}{8F_\pi^2 \kappa_v(m_\pi) \pi m_\pi} \\
& + \frac{c_A^2 M_N}{9F_\pi^2 \kappa_v(m_\pi) \pi^2 \sqrt{\Delta^2 - m_\pi^2}} \log \left[ \frac{\Delta}{m_\pi} + \sqrt{\frac{\Delta^2}{m_\pi^2} - 1} \right] \\
& + \frac{24M_N}{\kappa_v(m_\pi)} B_{c2}.
\end{aligned} \tag{6.14}$$

The leading non-analytic quark-mass dependence  $\sim m_\pi^{-1}$  is generated via the Goldstone boson cloud around a nucleon (diagrams (a)-(f) of Fig. 6), whereas the corresponding diagrams with an intermediate  $\Delta(1232)$  state (diagrams (g)-(k) in Fig. 6) produce the remaining quark-mass dependence.

At leading one-loop order, in standard chiral counting one would not encounter the term  $\propto B_{c2}$  (see Eq. (6.4)) which parametrises the short-distance (“core”) contributions to the Pauli radius analogous to  $B_{10}^{(r)}(\lambda)$  in the Dirac radius (6.12). However, such a term – which should be present according to the physics reasoning alluded to above – is known to exist, see term no. 54 in Ref. [26]. Utilizing the parameters of Table 4 one finds (for the physical pion mass) the following contributions to the radius:

$$(r_2^v)^2 = (0.53 (N\pi) + 0.09 (\Delta\pi) + 0.24 \text{ GeV}^3 B_{c2}) \text{ fm}^2, \tag{6.15}$$

which without the “core term”  $\propto B_{c2}$  are too small by 20% when compared to the empirical value  $(r_2^v)_{\text{exp}}^2 = 0.797 \text{ fm}^2$  [23]. Setting  $B_{c2} = 0.74 \text{ GeV}^{-3}$  for the physical parameters considered here (see Table 4) one can reproduce the dispersion theoretical result with a *positive* core contribution. We shall study the chiral extrapolation function of  $(r_2^v)^2$  with and without this core term in Section 7.2 to test whether our physical intuition regarding this structure holds true.

The radii display much fewer quark-mass dependent terms than  $\kappa_v(m_\pi)$  in Eq. (6.6) though all three quantities are calculated to the same  $\mathcal{O}(\epsilon^3)$  accuracy in SSE. This seems to have its origin in the fact that one has to take out a factor of  $q^2$  from the  $\mathcal{O}(\epsilon^3)$  expression for the form factors in Eqs. (6.3), (6.4) in order to obtain the radius, leaving only a few possible structures for quark-mass dependent terms at this order. From the point of view of ChEFT it is therefore more involved to get the quark-mass dependence of radii under control than it is to study the quark-mass dependence of the form factors at  $q^2 = 0$ . In Section 7 we shall compare the ChEFT formulae with the lattice data.

Even without the additional core term in Eq. (6.14) the dipole formulae with the above expressions for the radii reproduce the dispersion-theoretical form factors quite accurately for small and moderate values of  $Q^2$  as can be seen



Table 5

Fit values from fits of Eqs. (6.6) and (7.1) to lattice data.

Parameter	Value from Ref. [18]	Fit value (this work)
$\kappa_v^0$	5.1(4)	4.7(9)
$c_V$	$-2.26(6) \text{ GeV}^{-1}$	$-2.8(6) \text{ GeV}^{-1}$
$E_1^{(r)}(0.6 \text{ GeV})$	$-4.93(10) \text{ GeV}^{-3}$	$-5.8(9) \text{ GeV}^{-3}$
$\kappa_s^0$	-0.11	-0.24(15)
$E_2$	$0.074 \text{ GeV}^{-3}$	$0.04(3) \text{ GeV}^{-3}$

from the dashed curves in Fig. 7. This observation constitutes a further argument in favour of our dipole fits. Empirical isovector dipole masses can be computed from the phenomenological isovector radii. One finds  $M_e^v = 0.75 \text{ GeV}$  and  $M_m^v = 0.79 \text{ GeV}$ .

A final remark concerns the applicability of the above formulae to quenched data. Obviously, standard ChEFT presupposes the presence of sea quarks. However, as first unquenched simulations show, there is little difference between quenched and unquenched results at presently accessible quark masses. It is therefore not unreasonable to compare (6.3), (6.4) and (6.6) with quenched data. Alternatively, one could try to develop quenched chiral perturbation theory for the form factors. For first attempts see, e.g., Refs. [15,27].

## 7 Comparison with chiral effective field theory

### 7.1 Comparison with previous parametrisations for $\kappa_v(m_\pi)$

Hemmert and Weise [18] fitted lattice results for the isovector anomalous magnetic moment  $\kappa_v$  with formula (6.6) using  $\kappa_v^0$ ,  $c_V$  and  $E_1^{(r)}(\lambda)$  as fit parameters and fixing the other parameters at their phenomenological values (see Table 4). Their fit yielded a rather strong  $m_\pi$  dependence of  $\kappa_v$  for small  $m_\pi$ . The values they obtained for their fit parameters are given in the second column of Table 5. A similarly strong  $m_\pi$  dependence had already been observed in Refs. [19,20] for the magnetic moments of the proton and the neutron.

We have performed the same fit with our data for  $m_\pi < 1 \text{ GeV}$  and found the fit parameters given in the third column of Table 5. In Fig. 8 we plot our (normalised) data together with our fit curve. For comparison we also show the curve corresponding to the parameters obtained in Ref. [18], which indicates that the  $\kappa_v$  data used in Ref. [18] lie somewhat below ours.

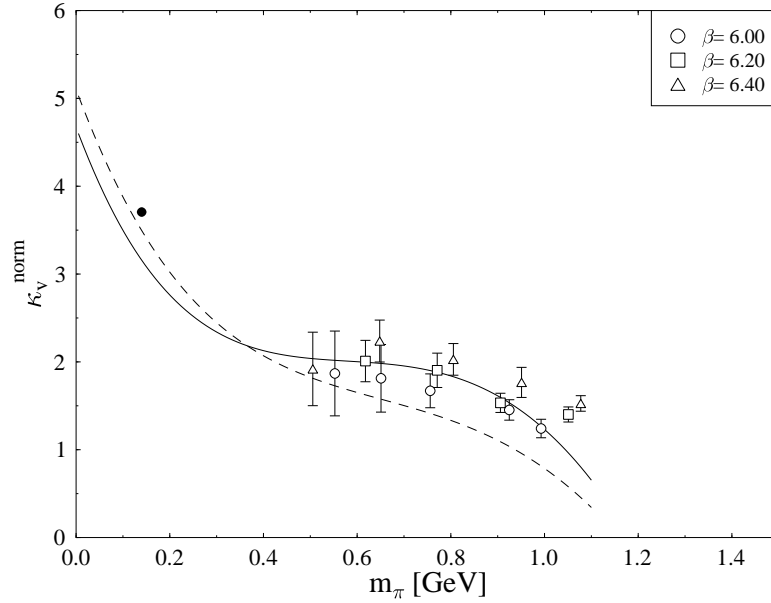


Fig. 8. Isovector (normalised) anomalous magnetic moments compared with our SSE fit (solid line). The dashed line is the SSE curve with the parameters taken from Ref. [18]. The solid circle represents the experimental value of  $\kappa_v$ .

## 7.2 Combined fits

The SSE curve for the isovector anomalous magnetic moment shown in Fig. 8 is compatible both with the experimental value and the lattice data. Of course, one has to remember that some of the parameters used in this curve were determined from a fit to lattice data. This raises the question whether one could not obtain a similarly good description of the radii by fitting the SSE expression to the simulation results. From the point of view of ChEFT the mass dependence of the Dirac and Pauli radius is much simpler to discuss than that of the analogous Sachs quantities. Hence we shall base our analysis on  $r_1^v$  and  $r_2^v$  instead of  $M_e^v$  and  $M_m^v$ .

Because cut-off effects seem to be small we fitted the results from all three  $\beta$  values together taking into account all data points with  $m_\pi < 1$  GeV. We kept  $F_\pi$ ,  $M_N$ ,  $c_A$  and  $\Delta$  at their phenomenological values (see Table 4), fixed the renormalisation scale  $\lambda$  at 0.6 GeV and chose  $B_{10}^{(r)}(0.6 \text{ GeV}) = 0$  for the reason explained in Section 6.2. Furthermore, we set  $g_A = 1.2$ , which is the value in the chiral limit obtained in a recent ChEFT analysis [28] of quenched lattice data. This leaves us with four fit parameters:  $\kappa_v^0$ ,  $c_V$ ,  $E_1^{(r)}(0.6 \text{ GeV})$  and  $B_{c2}$ . As the Dirac radius  $r_1^v$  is independent of these parameters, we performed a simultaneous fit of  $(r_2^v)^2(m_\pi)$  and  $\kappa_v(m_\pi)$ . The results are collected in the

second column of Table 6 and plots of our data together with the fit curves are shown in Figs. 9, 10. Leaving out the core term in  $R_2^v$ , i.e. setting  $B_{c2} = 0$ , leads to the parameter values given in the third column of Table 6. The corresponding curves are shown as dashed lines in the figures.

Table 6

Results of a combined fit (with and without core term) of isovector Pauli radii and anomalous magnetic moments.

Parameter	Fitted value	Fitted value without core term
$\kappa_v^0$	5.1(7)	4.9(8)
$c_V$	$-2.1(5) \text{ GeV}^{-1}$	$-2.1(5) \text{ GeV}^{-1}$
$E_1^{(r)}(0.6 \text{ GeV})$	$-4.4(7) \text{ GeV}^{-3}$	$-4.4(8) \text{ GeV}^{-3}$
$B_{c2}$	$0.23(3) \text{ GeV}^{-3}$	$0.0 \text{ GeV}^{-3}$

The lattice data for the isovector anomalous magnetic moment are very well described by the chiral extrapolation curve, in particular if one allows for a (small) core contribution via  $B_{c2}$ . Interestingly, the chiral extrapolation function comes rather close to the physical point, although the lightest lattice points are quite far from the physical world and large curvature is required. Moreover, the chiral limit value  $\kappa_v^0 = 5.1 \pm 0.7$  and the values of the other two fit parameters  $E_1^{(r)}$  and  $c_V$  compare astonishingly well with the numbers found in Ref. [18] providing us with some confidence in their determination. The lattice data for the isovector Pauli radius (squared) are also reasonably well described by the chiral extrapolation function of Eq. (6.14), at least for pion masses below 800 MeV. The effect of the finite core size of the nucleon (parametrised via  $B_{c2}$ ) is more visible in this quantity than in  $\kappa_v$ . While the phenomenological value at the physical point is missed by our central curve for  $r_2^v(m_\pi)$ , it would lie within the error band, given the relatively large errors of the fit parameters. We note that the  $1/m_\pi$  chiral singularity shows up rather strongly, dominating the curvature out to pion masses around 0.3 GeV.

While our generalisation of the ChEFT analysis of Ref. [18] describes the “magnetic” quantities  $\kappa_v$  and  $r_2^v$  reasonably well, it is not successful for the isovector Dirac radius. As can be seen in Fig. 9, the chiral extrapolation function drops too fast with  $m_\pi$  and even reaches zero around  $m_\pi = 1 \text{ GeV}$ . Remember that Dirac radius data were not included in the fit and the curve shown corresponds to the “no-core term” scenario with  $B_{10}^{(r)}(\lambda = 0.6 \text{ GeV}) = 0$ . One could improve the agreement between the lattice data and the chiral extrapolation curve by allowing  $B_{10}^{(r)}$  to provide a positive core contribution, which would shift the curve upwards towards the data. However, this would result in extremely large values for  $(r_1^v)^2$  at the physical point, as the shape

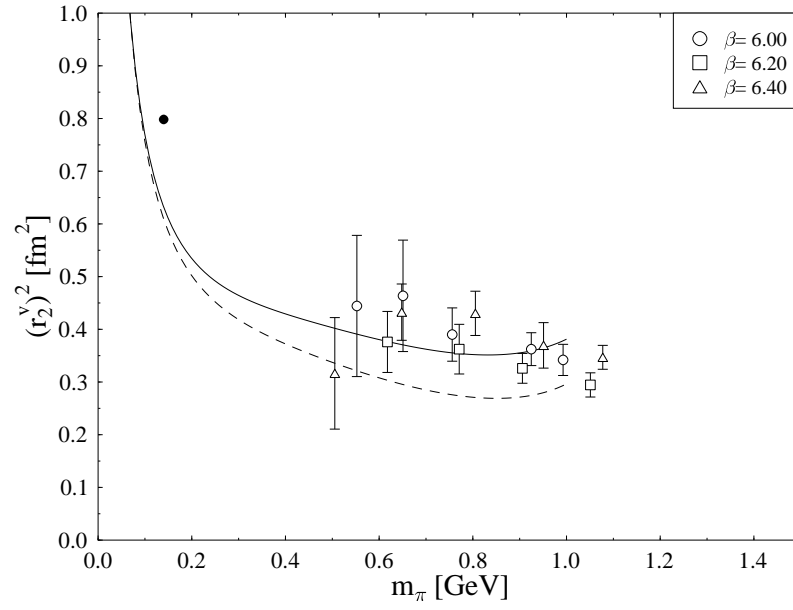
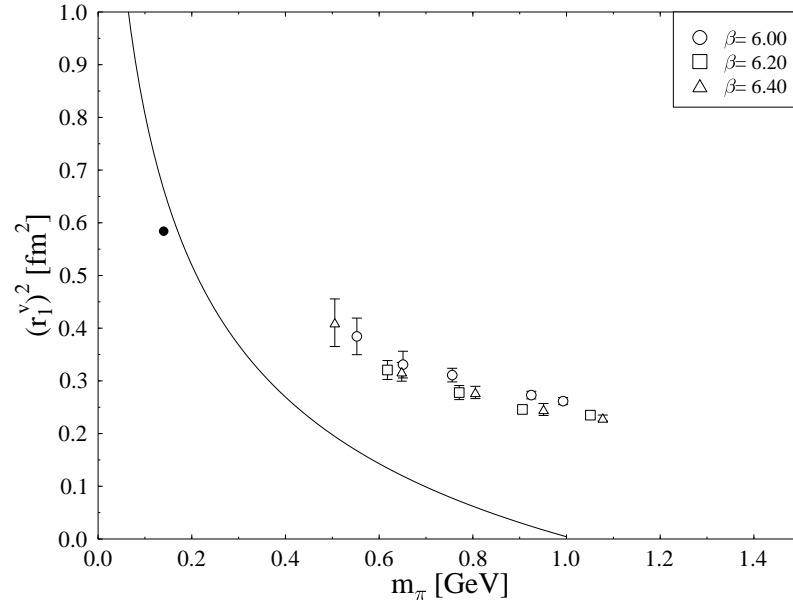


Fig. 9. Isovector radii compared with fit curves. For the fit parameters see Table 6. The dashed line corresponds to the fit without core term. The solid circles represent the experimental values.

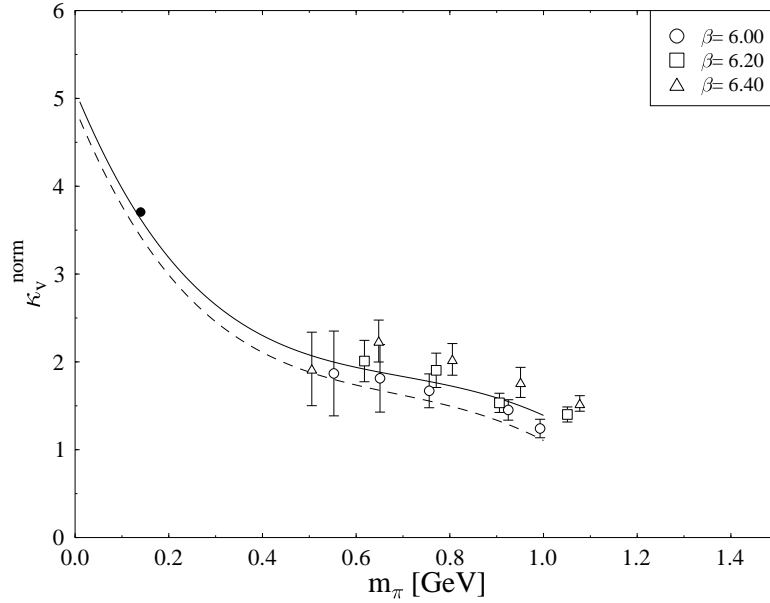


Fig. 10. Isovector (normalised) anomalous magnetic moments compared with (combined) fit. For the fit parameters see Table 6. The dashed line corresponds to the fit without core term. The solid circle represents the experimental value of  $\kappa_v$ .

is not modified by  $B_{10}^{(r)}$ . On the other hand, the simulation data themselves look completely reasonable, indicating that for pion masses around 1 GeV, for which the pion cloud should be considerably reduced, the square of the Dirac radius of the nucleon has shrunk to  $\approx 0.25 \text{ fm}^2$ , less than half of the value at the physical point. One reason for this failure of Eq. (6.12) might lie in important higher order corrections in ChEFT which could soften the strong  $m_\pi$  dependence originating from the chiral logarithm.

Nevertheless, one should also not forget that here we are dealing with a quenched simulation. Given that  $(r_1^v)^2$  at the physical point is nearly completely dominated by the pion cloud (for low values of  $\lambda$ , cf. Eq. (6.13)) it is conceivable that the Dirac radius of the nucleon might be sensitive to the effects of (un)quenching. We therefore conclude that especially for  $r_1^v$  a lot of work remains to be done, both on the level of ChEFT, where the next-to-leading one-loop contributions need to be evaluated, as well as on the level of the simulations, where a similar analysis as the one presented here has to be performed based on fully dynamical configurations.

Of course, one can think of alternative fit strategies, which differ by the choice of the fixed parameters. For example, one might leave also  $c_A$  and  $\Delta$  free in addition to the four parameters used above. In this (or a similar) way it is possible to force the fit through the data points for  $(r_1^v)^2$  also, but then the

physical point is missed by a considerable amount. So we must conclude that at the present level of accuracy the SSE expression for the Dirac radius is not sufficient to connect the Monte Carlo data in a physically sensible way with the phenomenological value.

### 7.3 Beyond the isovector channel

While ChEFT (to the order considered in Ref. [18]) yields the rather intricate expression (6.6) for the quark-mass dependence of the isovector anomalous magnetic moment, the analogous expression for the isoscalar anomalous magnetic moment  $\kappa_s = \kappa_p + \kappa_n$  of the nucleon is much simpler,

$$\kappa_s(m_\pi) = \kappa_s^0 - 8E_2 M_N m_\pi^2, \quad (7.1)$$

because the Goldstone boson contributions to this quantity only start to appear at the two-loop level [29]. The new counterterm  $E_2$  parametrises quark-mass dependent short-distance contributions to  $\kappa_s$ . The error bars of the lattice data are quite large compared to the small isoscalar anomalous magnetic moment. Therefore, any analysis based on (7.1) and the present lattice results must be considered with great caution, the more so, since the lattice data are also afflicted with the problem of the disconnected contributions. In spite of all these caveats, we now turn to a discussion of the magnetic moments and combinations of them which are not purely isovector quantities.

In Fig. 11 we present the normalised values of  $\kappa_s$  together with a fit using Eq. (7.1). The values of  $\kappa_s$  have been computed as  $\kappa_p + \kappa_n$  from the proton and neutron dipole fits of  $G_m$ , and the errors have been determined by error propagation. The parameter values obtained in the fit are given in the third column of Table 5 while the second column contains the corresponding numbers from Ref. [18].

Having determined  $\kappa_v(m_\pi)$  as well as  $\kappa_s(m_\pi)$  we can now discuss the chiral extrapolation of proton and neutron data separately. For  $\kappa_v^0$ ,  $c_V$ ,  $E_1^{(r)}$ ,  $B_{c2}$  we choose the values given in the second column of Table 6 together with  $g_A = 1.2$ ,  $\kappa_s^0$  and  $E_2$  are taken from the third column of Table 5, and the remaining parameters are fixed at their physical values (see Table 4).

In Fig. 12 we compare the resulting extrapolation functions with the lattice results for the total magnetic moments. The extrapolation functions are surprisingly well behaved. Despite the large gap between  $m_\pi^{\text{phys}}$  and the lowest data point and the substantial curvature involved they extrapolate to the physical point and to the chiral limit in a very sensible way.

Finally, we want to compare our results with the predictions from the con-

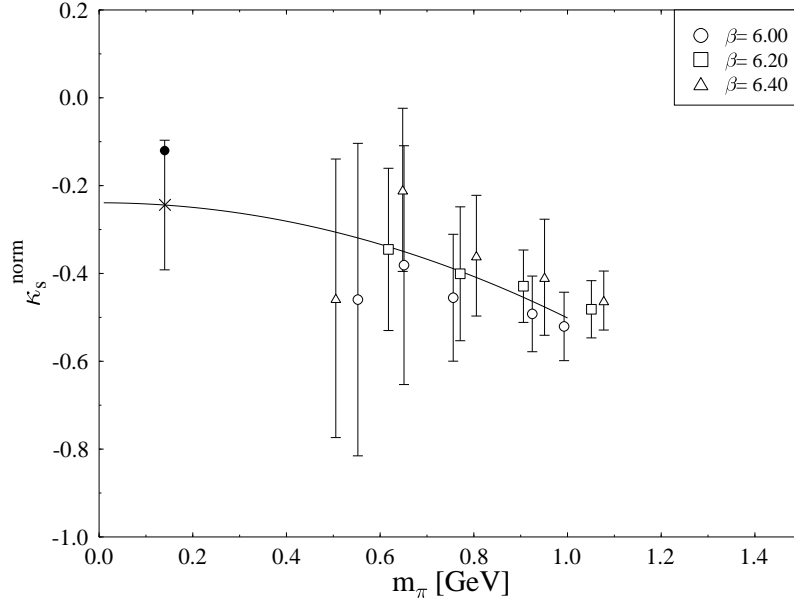


Fig. 11. Isoscalar (normalised) anomalous magnetic moments compared with SSE fit. The solid circle represents the experimental value of  $\kappa_s$ .

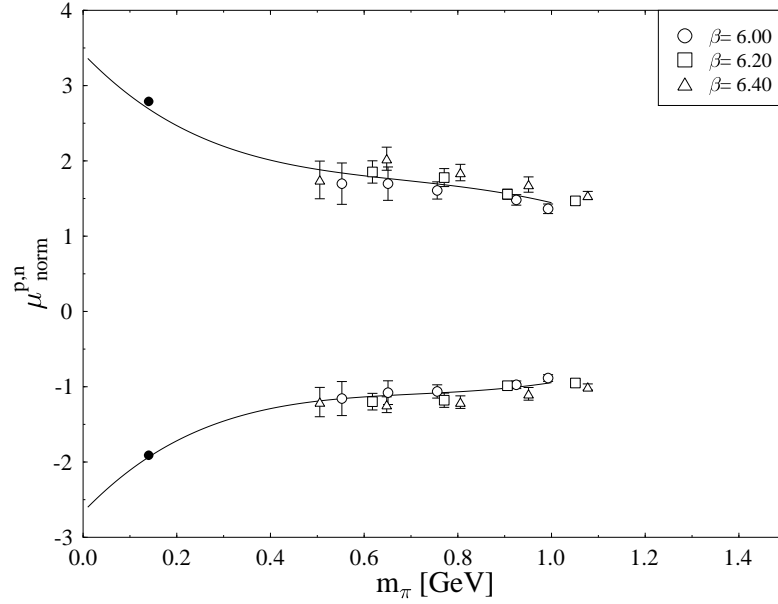


Fig. 12. Magnetic moments of proton and neutron with chiral extrapolation curves. The solid circles represent the experimental values.

stituent quark model. Such comparisons are usually performed for ratios of observables to avoid normalisation problems. In Fig. 13 we show the ratio of the total magnetic moments  $\mu^p/\mu^n$  as a function of the pion mass. Surprisingly, the lattice data and our extrapolation function stay rather close to the static SU(6) quark model value of  $-3/2$  in the mass range considered here. However, given the size of the lattice error bars no conclusions can be drawn about a possible “restoration” of the quark model for large pion masses as advocated in Ref. [20]. On the other hand, the static quark model would also predict  $\kappa_p/\kappa_n = -1$  for the ratio of the anomalous magnetic moments shown in Fig. 14. Here we see a clear trend away from the quark-model result as the quark mass increases, consistent with the observation already made in Ref. [18].

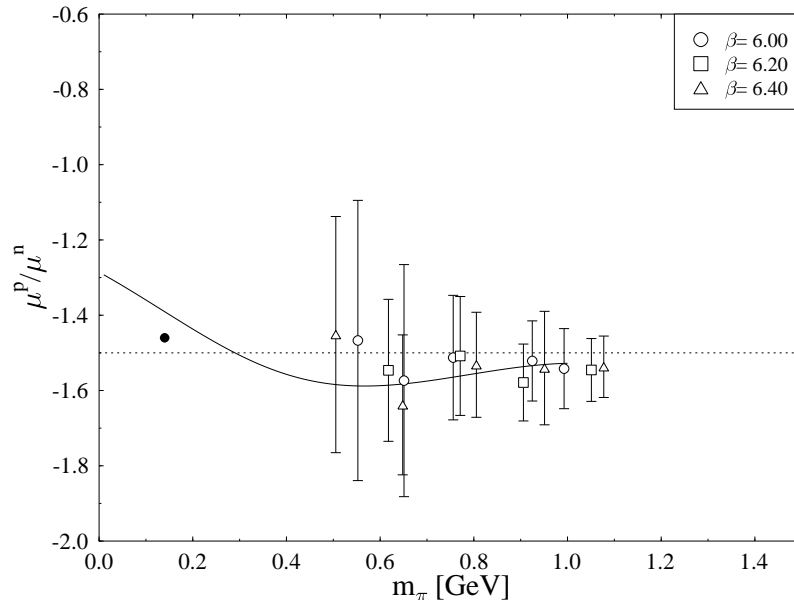


Fig. 13. The ratio  $\mu^p/\mu^n$  with chiral extrapolation curve. The dotted line shows the value  $-1.5$  predicted by the non-relativistic quark model. The solid circle represents the experimental value.

## 8 Conclusions

We have performed a detailed study of the electromagnetic nucleon form factors within quenched lattice QCD employing a fully non-perturbative  $O(a)$ -improvement of the fermionic action and of the electromagnetic current. Compared with previous studies [4,5] we have accumulated much higher statistics, yet our statistical errors appear to be rather large. While these older investigations used one lattice spacing only, we have data at three different lattice



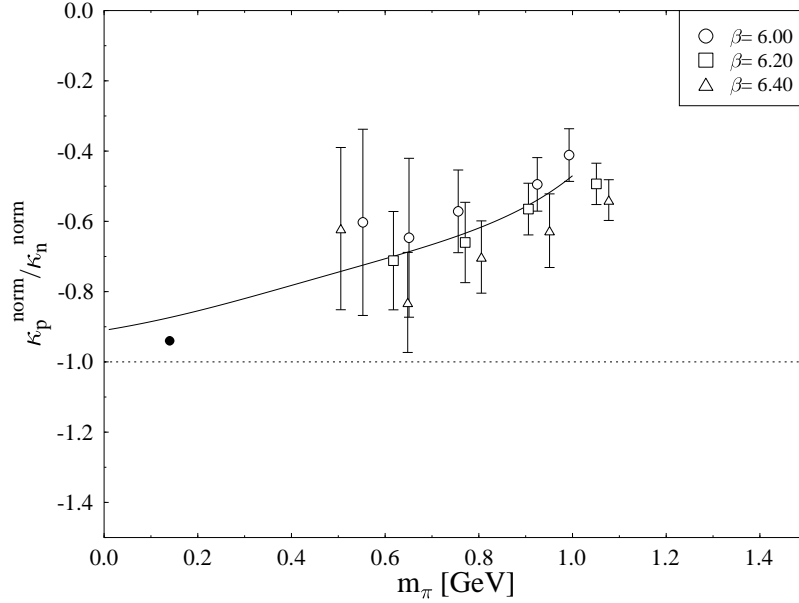


Fig. 14. The ratio  $\kappa_p/\kappa_n$  with chiral extrapolation curve. The dotted line shows the value  $-1.0$  predicted by the non-relativistic quark model. The solid circle represents the experimental value.

spacings. So we could study the discretisation errors and found them to be small.

As the quark masses in our simulations are considerably larger than in reality, we had to deal with chiral extrapolations. The most effective way to handle this problem proceeds via a suitable parametrisation of the  $Q^2$  dependence of the form factors. Indeed, our data can be described reasonably well by dipole fits. Then the quark-mass dependence of the fit parameters (dipole masses, in particular) can be studied. Assuming a linear dependence on the pion mass one ends up remarkably close to the physical values, in spite of the fact that the singularities arising from the Goldstone bosons of QCD must show up at some point invalidating such a simple picture. Nevertheless, the difference between the electric and the magnetic dipole mass which we obtain at the physical pion mass is in (semi-quantitative) agreement with recent experimental results [2,3].

Ideally, the chiral extrapolation should be guided by ChEFT. However, most of the existing chiral expansions do not take into account quenching artefacts and are therefore, strictly speaking, not applicable to our data. But first simulations with dynamical quarks indicate that at the quark masses considered in this paper quenching effects are small so that quenched chiral perturbation theory is not required. While in this respect the size of our quark masses might be helpful, it leads on the other hand to doubts on the applicability of ChEFT.

Indeed, only a reorganisation of the standard chiral perturbation theory series allowed Hemmert and Weise [18] to describe with a single expression the phenomenological value of the isovector anomalous magnetic moment of the nucleon as well as (quenched) lattice data. For a different approach to the same problem see Refs. [19,20].

We have extended the analysis of the magnetic moments of the nucleon of Ref. [18] to the general case of nucleon electromagnetic form factors. Given that these calculations are reliable only for  $Q^2 < 0.4 \text{ GeV}^2$ , no direct comparison with our lattice data, taken at higher values of  $Q^2$ , could be performed. Instead we have converted the dipole masses extracted from our simulations into form factor radii, which could then be compared with the ChEFT formulae. Larger lattices allowing smaller values of  $Q^2$  would be required, if one aims at a direct comparison with the ChEFT results for the form factors.

In the isovector channel a combined fit of  $\kappa_v(m_\pi)$  and the Pauli radius  $r_2^v(m_\pi)$  yielded extrapolation functions which describe the lattice data quite well and extrapolate (albeit with large error bar) close to the physical point. For the isovector Dirac radius  $r_1^v(m_\pi)$  no chiral extrapolation function could be obtained that is consistent both with the lattice data and known phenomenology at the physical point. Further studies are needed to resolve this discrepancy, both in ChEFT regarding higher order corrections and on the simulation side investigating quenching effects. (For an alternative view see Ref. [21].) The parameters obtained in the fits are well consistent with those found in Ref. [18]. In particular, we find  $\kappa_v^0 = 5.1 \pm 0.7$  as the chiral limit value for the isovector anomalous magnetic moment of the nucleon.

The isoscalar sector is plagued by large uncertainties in the lattice data. The chiral dynamics contributing to extrapolation functions in this sector seems to be dominated by analytic terms. Quantitative studies can only be performed once the statistics of the data is improved and disconnected contributions are taken into account.

The leading one-loop calculation in the SSE is found to describe the quark-mass dependence of magnetic quantities quite well. Unfortunately, at the moment we do not have a ChEFT with appropriate counting scheme that simultaneously describes the quark-mass dependence in all four quantities  $\kappa_v$ ,  $\kappa_s$ ,  $r_1^v$ ,  $r_2^v$  at leading one-loop order. It remains to be seen whether the discrepancies found in  $r_1^v(m_\pi)$  can be resolved in a next-to-leading one-loop SSE calculation of the form factors. The figures in this paper show that ChEFT often predicts large effects at values of  $m_\pi$  lighter than those we used in our lattice simulations. In order to confirm the predictions of ChEFT, and in order to extrapolate reliably to physical quark masses, we need simulations at much smaller values of  $m_\pi$ . Moreover, it would be desirable to compute the quark-line disconnected contributions. Important progress is also to be expected from

the ongoing simulations with dynamical fermions.

## Acknowledgements

This work has been supported in part by the European Community's Human Potential Program under contract HPRN-CT-2000-00145, Hadrons/Lattice QCD, by the DFG (Forschergruppe Gitter-Hadronen-Phänomenologie) and by the BMBF. Discussions with V. Braun and W. Weise are gratefully acknowledged. TRH thanks the Institute for Theoretical Physics of the University of Regensburg and DESY Zeuthen for their kind hospitality.

The numerical calculations were performed on the APE100 at NIC (Zeuthen) as well as on the Cray T3E at ZIB (Berlin) and NIC (Jülich). We wish to thank all institutions for their support.

## Appendix A

In this Appendix we collect our results for the nucleon form factors.

Table 7

Isovector nucleon form factors at  $\beta = 6.0$ .

$\kappa$	$a^2 Q^2$	$G_e$	$G_m$	$F_1$	$F_2$
0.1320	0.0000	0.9962(6)		0.9962(6)	
	0.1484	0.554(7)	2.34(4)	0.621(7)	1.72(4)
	0.1492	0.56(2)	2.4(2)	0.63(2)	1.8(2)
	0.2867	0.42(3)	1.69(17)	0.51(3)	1.18(16)
	0.3084	0.357(14)	1.50(8)	0.443(14)	1.06(8)
	0.4168	0.30(5)	1.3(2)	0.40(5)	0.88(18)
	0.4576	0.28(2)	1.13(8)	0.37(2)	0.76(8)
	0.6169	0.141(9)	0.67(4)	0.215(9)	0.45(3)
0.1324	0.0000	0.9936(7)		0.9936(7)	
	0.1480	0.544(7)	2.40(4)	0.619(7)	1.78(4)
	0.1488	0.60(2)	2.6(2)	0.68(2)	1.88(19)
	0.2852	0.40(3)	1.64(16)	0.49(3)	1.15(15)
	0.3084	0.327(14)	1.41(9)	0.415(14)	1.00(8)
	0.4137	0.26(3)	1.39(17)	0.38(4)	1.01(16)
	0.4573	0.27(2)	1.10(9)	0.36(2)	0.73(8)
	0.5350	0.108(18)	0.59(12)	0.17(2)	0.42(11)
	0.6169	0.131(8)	0.69(4)	0.216(9)	0.48(3)
0.1333	0.0000	0.9921(18)		0.9921(18)	
	0.1463	0.503(10)	2.21(6)	0.590(9)	1.62(5)
	0.1477	0.58(4)	2.6(4)	0.68(4)	2.0(4)
	0.2796	0.37(4)	1.5(2)	0.48(4)	1.0(2)
	0.3084	0.28(2)	1.21(12)	0.38(2)	0.83(11)
	0.4029		1.3(2)		
	0.4561	0.24(5)	1.02(15)	0.35(4)	0.67(13)
	0.6169	0.099(11)	0.59(5)	0.191(13)	0.40(4)
0.1338	0.0000	0.999(4)		0.999(4)	
	0.1447	0.475(14)	1.94(8)	0.566(14)	1.38(8)
	0.2741	0.30(6)	0.8(2)	0.36(6)	0.5(2)
	0.3084	0.28(3)	1.17(16)	0.39(3)	0.78(14)
	0.6169	0.12(2)	0.49(6)	0.20(2)	0.29(5)
0.1342	0.0000	0.987(6)		0.987(6)	
	0.1439	0.437(17)	1.91(9)	0.535(17)	1.38(9)
	0.3084	0.26(4)	0.98(17)	0.35(4)	0.62(15)
	0.6169		0.49(8)		

Table 8  
Isovector nucleon form factors at  $\beta = 6.2$ .

$\kappa$	$a^2 Q^2$	$G_e$	$G_m$	$F_1$	$F_2$
0.1333	0.0000	1.0010(2)		1.0010(2)	
	0.0665	0.621(7)	3.03(5)	0.692(7)	2.34(5)
	0.0667	0.615(18)	2.90(17)	0.683(18)	2.21(16)
	0.1294	0.413(18)	2.03(11)	0.504(18)	1.52(10)
	0.1371	0.407(15)	2.04(10)	0.504(15)	1.53(10)
	0.1892	0.34(4)	1.62(17)	0.44(4)	1.18(16)
	0.2038	0.32(2)	1.58(8)	0.43(2)	1.15(8)
	0.2742	0.206(10)	1.10(5)	0.306(11)	0.79(5)
0.1339	0.0000	1.0009(3)		1.0009(3)	
	0.0661	0.597(7)	2.77(5)	0.676(7)	2.10(5)
	0.0664	0.64(2)	2.7(2)	0.71(2)	2.0(2)
	0.1279	0.44(3)	2.0(2)	0.55(3)	1.50(19)
	0.1371	0.406(16)	1.84(9)	0.510(16)	1.34(8)
	0.2035	0.32(2)	1.34(9)	0.43(2)	0.92(8)
	0.2742	0.176(11)	0.95(5)	0.279(12)	0.67(4)
0.1344	0.0000	1.0031(7)		1.0031(7)	
	0.0655	0.562(11)	2.74(7)	0.658(11)	2.08(7)
	0.0660	0.56(4)	2.8(3)	0.66(4)	2.1(3)
	0.1259	0.35(3)	1.64(15)	0.46(3)	1.19(14)
	0.1371	0.35(2)	1.65(14)	0.46(2)	1.19(13)
	0.2031	0.28(4)	1.43(14)	0.43(3)	1.00(12)
	0.2742	0.162(15)	0.87(7)	0.277(17)	0.59(6)
0.1349	0.0000	1.0052(18)		1.0052(18)	
	0.0647	0.525(12)	2.44(7)	0.631(12)	1.81(7)
	0.0654	0.55(5)	2.8(4)	0.67(5)	2.1(4)
	0.1233	0.30(4)	1.44(19)	0.42(4)	1.02(18)
	0.1371	0.31(3)	1.41(14)	0.44(3)	0.97(13)
	0.2025	0.26(4)	1.24(14)	0.42(4)	0.82(13)
	0.2742	0.123(18)	0.75(7)	0.25(2)	0.51(6)

Table 9

Isovector nucleon form factors at  $\beta = 6.4$ .

$\kappa$	$a^2Q^2$	$G_e$	$G_m$	$F_1$	$F_2$
0.1338	0.0000	1.0019(18)		1.0019(18)	
	0.0375	0.636(6)	3.10(5)	0.705(6)	2.40(5)
	0.0376	0.626(16)	3.05(14)	0.693(16)	2.36(14)
	0.0730	0.413(18)	1.95(10)	0.494(18)	1.45(10)
	0.0771	0.416(13)	2.10(8)	0.510(13)	1.59(7)
	0.1069	0.29(2)	1.34(9)	0.37(2)	0.97(9)
	0.1147	0.30(2)	1.48(7)	0.397(19)	1.09(7)
	0.1394	0.21(2)	1.00(14)	0.29(2)	0.71(13)
	0.1542	0.215(11)	1.13(5)	0.311(11)	0.82(5)
0.1342	0.0000	1.002(5)		1.002(5)	
	0.0373	0.611(11)	3.01(8)	0.689(11)	2.32(7)
	0.0374	0.61(3)	3.0(2)	0.69(3)	2.3(2)
	0.0724	0.44(4)	2.2(2)	0.55(4)	1.7(2)
	0.0771	0.38(2)	2.05(14)	0.49(2)	1.56(13)
	0.1145	0.26(3)	1.38(11)	0.36(3)	1.02(11)
	0.1542	0.171(19)	0.93(8)	0.26(2)	0.66(8)
0.1346	0.0000	1.003(5)		1.003(5)	
	0.0370	0.576(10)	2.77(6)	0.665(10)	2.11(6)
	0.0372	0.54(3)	2.8(3)	0.63(3)	2.1(3)
	0.0713	0.34(3)	1.53(13)	0.43(3)	1.10(12)
	0.0771	0.347(19)	1.71(10)	0.457(19)	1.25(9)
	0.1034	0.23(4)	1.09(14)	0.32(4)	0.76(13)
	0.1143	0.28(4)	1.24(10)	0.39(4)	0.85(10)
	0.1338	0.16(4)	0.71(14)	0.23(4)	0.48(13)
	0.1542	0.163(14)	0.90(6)	0.273(15)	0.63(5)
0.1350	0.0000	1.006(8)		1.006(8)	
	0.0366	0.531(12)	2.60(8)	0.636(12)	1.97(7)
	0.0369	0.48(5)	2.6(4)	0.59(6)	2.0(4)
	0.0700	0.32(4)	1.57(19)	0.44(4)	1.13(18)
	0.0771	0.29(3)	1.58(15)	0.42(3)	1.16(13)
	0.1009		1.2(3)		
	0.1140	0.26(5)	1.11(12)	0.38(5)	0.73(11)
	0.1298		0.69(17)		
	0.1542	0.142(17)	0.78(6)	0.259(18)	0.53(5)
0.1353	0.0000	1.006(7)		1.006(7)	
	0.0360	0.48(2)	2.22(14)	0.59(2)	1.63(13)
	0.0681		1.5(3)		
	0.0771	0.24(5)	1.39(18)	0.39(5)	1.00(17)
	0.1542		0.73(11)		

Table 10  
Proton form factors at  $\beta = 6.0$ .

$\kappa$	$a^2 Q^2$	$G_e$	$G_m$	$F_1$	$F_2$
0.1320	0.0000	0.9980(5)		0.9980(5)	
	0.1484	0.566(6)	1.43(3)	0.599(6)	0.83(3)
	0.1492	0.58(2)	1.49(13)	0.61(2)	0.88(13)
	0.2867	0.42(2)	1.02(10)	0.47(2)	0.56(10)
	0.3084	0.372(12)	0.91(5)	0.413(11)	0.50(5)
	0.4168	0.34(5)	0.77(12)	0.38(4)	0.39(12)
	0.4576	0.287(19)	0.70(5)	0.332(18)	0.37(5)
	0.6169	0.153(8)	0.41(2)	0.190(7)	0.22(2)
0.1324	0.0000	0.9964(6)		0.9964(6)	
	0.1480	0.557(6)	1.47(3)	0.594(5)	0.87(3)
	0.1488	0.600(19)	1.59(13)	0.640(19)	0.95(13)
	0.2852	0.40(2)	1.02(10)	0.45(2)	0.57(9)
	0.3084	0.340(11)	0.88(5)	0.384(11)	0.49(5)
	0.4137	0.29(3)	0.84(10)	0.34(3)	0.49(10)
	0.4573	0.267(18)	0.68(6)	0.315(17)	0.37(5)
	0.5350	0.118(17)	0.37(8)	0.152(18)	0.22(7)
0.1333	0.0000	0.9957(13)		0.9957(13)	
	0.1463	0.517(8)	1.36(3)	0.560(8)	0.80(3)
	0.1477	0.57(3)	1.6(2)	0.62(3)	1.0(2)
	0.2796	0.39(3)	0.91(14)	0.44(3)	0.47(13)
	0.3084	0.294(15)	0.76(7)	0.342(15)	0.42(7)
	0.4029	0.27(5)	0.81(15)	0.34(5)	0.47(14)
	0.4561	0.26(4)	0.66(9)	0.32(3)	0.34(9)
	0.6169	0.113(9)	0.37(3)	0.161(9)	0.21(3)
0.1338	0.0000	1.000(3)		1.000(3)	
	0.1447	0.488(12)	1.21(5)	0.532(11)	0.67(5)
	0.2741	0.30(5)	0.54(15)	0.32(5)	0.22(14)
	0.3084	0.30(2)	0.74(10)	0.35(2)	0.39(9)
	0.6169	0.125(17)	0.31(4)	0.166(16)	0.14(3)
0.1342	0.0000	0.994(5)		0.994(5)	
	0.1439	0.451(13)	1.17(6)	0.499(13)	0.68(6)
	0.3084	0.25(3)	0.62(11)	0.30(3)	0.32(10)
	0.6169	0.094(19)	0.31(5)	0.145(19)	0.17(4)

Table 11  
Proton form factors at  $\beta = 6.2$ .

$\kappa$	$a^2Q^2$	$G_e$	$G_m$	$F_1$	$F_2$
0.1333	0.0000	1.00196(17)		1.00196(17)	
	0.0665	0.633(5)	1.85(3)	0.669(5)	1.18(3)
	0.0667	0.626(15)	1.82(11)	0.662(15)	1.16(10)
	0.1294	0.426(15)	1.24(7)	0.472(15)	0.77(6)
	0.1371	0.423(12)	1.24(6)	0.471(12)	0.77(6)
	0.1892	0.37(4)	1.00(11)	0.42(4)	0.58(10)
	0.2038	0.333(18)	0.97(5)	0.387(17)	0.58(5)
	0.2742	0.219(10)	0.67(3)	0.269(9)	0.40(3)
0.1339	0.0000	1.0020(3)		1.0020(3)	
	0.0661	0.607(6)	1.70(3)	0.646(6)	1.05(3)
	0.0664	0.637(19)	1.71(13)	0.676(19)	1.04(12)
	0.1279	0.45(3)	1.22(12)	0.50(3)	0.72(12)
	0.1371	0.414(13)	1.13(6)	0.466(13)	0.66(5)
	0.2035	0.33(2)	0.83(5)	0.380(19)	0.45(5)
	0.2742	0.184(10)	0.58(3)	0.237(9)	0.34(3)
0.1344	0.0000	1.0037(5)		1.0037(5)	
	0.0655	0.576(8)	1.67(4)	0.624(8)	1.05(4)
	0.0660	0.56(3)	1.8(2)	0.62(3)	1.1(2)
	0.1259	0.37(2)	1.02(9)	0.42(2)	0.60(9)
	0.1371	0.368(18)	1.00(8)	0.424(18)	0.57(8)
	0.1823	0.29(7)			
	0.2031	0.30(3)	0.88(8)	0.38(3)	0.50(8)
	0.2742	0.174(13)	0.53(4)	0.232(13)	0.30(4)
0.1349	0.0000	1.0054(12)		1.0054(12)	
	0.0647	0.535(9)	1.49(5)	0.588(9)	0.91(4)
	0.0654	0.55(4)	1.8(3)	0.62(4)	1.2(3)
	0.1233	0.34(3)	0.86(12)	0.39(3)	0.47(11)
	0.1371	0.34(2)	0.85(8)	0.392(19)	0.46(8)
	0.2025	0.27(4)	0.76(9)	0.34(3)	0.41(8)
	0.2742	0.133(13)	0.47(4)	0.199(13)	0.27(3)



Table 12  
Proton form factors at  $\beta = 6.4$ .

$\kappa$	$a^2Q^2$	$G_e$	$G_m$	$F_1$	$F_2$
0.1338	0.0000	1.0024(14)		1.0024(14)	
	0.0375	0.644(5)	1.89(3)	0.679(5)	1.21(3)
	0.0376	0.641(13)	1.89(9)	0.676(13)	1.21(9)
	0.0730	0.421(16)	1.19(6)	0.462(16)	0.73(6)
	0.0771	0.430(11)	1.30(5)	0.479(11)	0.82(5)
	0.1069	0.30(2)	0.82(6)	0.34(2)	0.48(6)
	0.1147	0.311(17)	0.91(5)	0.359(16)	0.55(4)
	0.1394	0.22(2)	0.61(9)	0.25(2)	0.36(8)
	0.1542	0.225(10)	0.69(3)	0.274(9)	0.42(3)
0.1342	0.0000	1.002(4)		1.002(4)	
	0.0373	0.622(9)	1.84(4)	0.661(9)	1.18(4)
	0.0374	0.60(2)	1.86(15)	0.65(2)	1.22(15)
	0.0724	0.45(3)	1.38(14)	0.50(3)	0.88(13)
	0.0771	0.398(19)	1.26(9)	0.454(19)	0.81(8)
	0.1145	0.27(3)	0.84(7)	0.32(2)	0.52(7)
	0.1542	0.186(17)	0.58(5)	0.234(16)	0.34(5)
0.1346	0.0000	1.003(3)		1.003(3)	
	0.0370	0.588(8)	1.70(4)	0.632(7)	1.06(4)
	0.0372	0.58(2)	1.72(17)	0.62(2)	1.10(17)
	0.0713	0.35(2)	0.95(8)	0.40(2)	0.55(8)
	0.0771	0.368(15)	1.07(6)	0.425(14)	0.65(6)
	0.1034	0.24(4)	0.67(9)	0.29(3)	0.38(8)
	0.1143	0.28(3)	0.76(7)	0.34(3)	0.42(7)
	0.1338	0.16(2)	0.44(9)	0.19(2)	0.24(8)
	0.1542	0.175(12)	0.55(4)	0.232(11)	0.32(3)
0.1350	0.0000	1.004(6)		1.004(6)	
	0.0366	0.549(10)	1.60(5)	0.602(9)	1.00(5)
	0.0369	0.53(4)	1.6(3)	0.59(4)	1.0(3)
	0.0700	0.32(3)	1.00(12)	0.38(3)	0.61(11)
	0.0771	0.319(19)	0.99(9)	0.387(19)	0.61(9)
	0.1009	0.21(4)	0.74(18)	0.27(4)	0.47(16)
	0.1140	0.27(4)	0.64(8)	0.32(4)	0.32(8)
	0.1298		0.41(10)		
	0.1542	0.150(13)	0.48(4)	0.210(13)	0.27(3)
0.1353	0.0000	1.002(5)		1.002(5)	
	0.0360	0.474(17)	1.38(9)	0.533(17)	0.85(8)
	0.0681	0.32(6)	1.0(2)	0.40(6)	0.6(2)
	0.0771	0.28(4)	0.85(11)	0.35(3)	0.50(10)
	0.1542	0.15(3)	0.48(7)	0.23(3)	0.25(6)

Table 13

Magnetic form factor of the neutron at  $\beta = 6.0$ .

$\kappa$	$a^2Q^2$	$G_m$
0.1320	0.1484	-0.908(18)
	0.2867	-0.67(7)
	0.3084	-0.58(3)
	0.4168	-0.50(8)
	0.4576	-0.42(4)
	0.6169	-0.256(14)
0.1324	0.1480	-0.928(17)
	0.1488	-1.01(11)
	0.2852	-0.62(6)
	0.3084	-0.53(4)
	0.4137	-0.55(7)
	0.4573	-0.40(4)
	0.5350	-0.21(5)
	0.6169	-0.264(15)
0.1333	0.1463	-0.85(2)
	0.2796	-0.55(9)
	0.3084	-0.45(5)
	0.4029	-0.53(10)
	0.6169	-0.220(18)
0.1338	0.1447	-0.74(3)
	0.3084	-0.44(7)
	0.6169	-0.18(3)
0.1342	0.1439	-0.73(4)
	0.3084	-0.36(7)
	0.6169	-0.18(3)

Table 14

Magnetic form factor of the neutron at  $\beta = 6.2$ .

$\kappa$	$a^2Q^2$	$G_m$
0.1333	0.0665	-1.186(19)
	0.0667	-1.10(8)
	0.1294	-0.79(4)
	0.1371	-0.80(4)
	0.1892	-0.61(7)
	0.2742	-0.43(2)
0.1339	0.0661	-1.07(2)
	0.1279	-0.83(8)
	0.1371	-0.71(4)
	0.2742	-0.37(2)
0.1344	0.0655	-1.07(3)
	0.1259	-0.62(6)
	0.1371	-0.65(6)
	0.2742	-0.34(3)
0.1349	0.0647	-0.94(3)
	0.1233	-0.58(9)
	0.1371	-0.55(6)
	0.2742	-0.29(3)

Table 15

Magnetic form factor of the neutron at  $\beta = 6.4$ .

$\kappa$	$a^2Q^2$	$G_m$
0.1338	0.0375	-1.208(19)
	0.0376	-1.20(7)
	0.0730	-0.75(4)
	0.0771	-0.80(3)
	0.1069	-0.53(4)
	0.1394	-0.39(6)
	0.1542	-0.44(2)
0.1342	0.0373	-1.17(3)
	0.0724	-0.81(9)
	0.0771	-0.79(6)
	0.1542	-0.35(3)
0.1346	0.0370	-1.07(3)
	0.0713	-0.58(5)
	0.0771	-0.64(4)
	0.1034	-0.42(5)
	0.1338	-0.28(6)
	0.1542	-0.35(2)
0.1350	0.0366	-1.00(3)
	0.0700	-0.58(8)
	0.0771	-0.59(6)
	0.1009	-0.44(11)
	0.1140	-0.37(6)
	0.1542	-0.31(2)
0.1353	0.0360	-0.85(6)
	0.0681	-0.52(12)
	0.0771	-0.55(9)
	0.1542	-0.25(4)

## Appendix B

The following tables contain the results of our dipole fits. The masses are given in lattice units.

Table 16

Dipole fits of the isovector form factors.

$\kappa$	$aM_e$	$A_m$	$aM_m$	$aM_1$	$A_2$	$aM_2$
$\beta = 6.0$						
0.1320	0.657(6)	4.3(2)	0.66(2)	0.756(7)	3.4(2)	0.61(3)
0.1324	0.637(5)	4.5(2)	0.64(2)	0.745(7)	3.6(2)	0.60(3)
0.1333	0.593(8)	4.3(3)	0.61(3)	0.705(9)	3.5(4)	0.56(4)
0.1338	0.570(12)	4.1(6)	0.57(5)	0.675(14)	3.4(7)	0.50(6)
0.1342	0.534(14)	4.0(7)	0.57(7)	0.633(17)	4(2)	0.44(15)
$\beta = 6.2$						
0.1333	0.493(4)	4.79(17)	0.507(16)	0.579(5)	3.87(18)	0.480(19)
0.1339	0.477(5)	4.6(2)	0.484(17)	0.566(6)	3.7(2)	0.45(2)
0.1344	0.441(6)	4.7(3)	0.46(2)	0.539(8)	3.9(4)	0.42(3)
0.1349	0.411(7)	4.3(3)	0.45(3)	0.511(9)	3.5(4)	0.41(3)
$\beta = 6.4$						
0.1338	0.375(3)	5.16(18)	0.358(10)	0.436(4)	4.19(19)	0.340(12)
0.1342	0.358(5)	5.2(3)	0.347(17)	0.422(7)	4.2(3)	0.33(2)
0.1346	0.333(4)	5.1(3)	0.322(14)	0.399(5)	4.2(3)	0.299(16)
0.1350	0.310(5)	4.8(4)	0.319(16)	0.384(7)	3.9(4)	0.30(2)
0.1353	0.282(11)	3.7(5)	0.35(4)	0.350(14)	2.9(9)	0.33(9)

Table 17

Dipole fits of the proton form factors.

$\kappa$	$aM_e$	$A_m$	$aM_m$	$aM_1$	$A_2$	$aM_2$
$\beta = 6.0$						
0.1320	0.673(5)	2.59(12)	0.66(2)	0.720(5)	1.62(14)	0.61(4)
0.1324	0.653(5)	2.71(13)	0.64(2)	0.706(5)	1.70(14)	0.61(3)
0.1333	0.608(6)	2.59(18)	0.62(3)	0.665(7)	1.61(19)	0.59(5)
0.1338	0.583(10)	2.5(3)	0.58(5)	0.635(10)	1.7(5)	0.51(8)
0.1342	0.543(11)	2.4(4)	0.59(7)	0.596(11)	1.5(4)	0.55(10)
$\beta = 6.2$						
0.1333	0.505(4)	2.93(10)	0.505(16)	0.547(4)	1.97(12)	0.48(2)
0.1339	0.485(4)	2.81(12)	0.483(17)	0.527(4)	1.83(13)	0.45(3)
0.1344	0.453(5)	2.87(19)	0.46(2)	0.501(6)	2.0(2)	0.42(3)
0.1349	0.420(5)	2.6(2)	0.44(3)	0.469(6)	1.7(2)	0.41(4)
$\beta = 6.4$						
0.1338	0.383(3)	3.15(11)	0.359(10)	0.412(3)	2.13(12)	0.340(15)
0.1342	0.366(4)	3.17(19)	0.349(17)	0.398(5)	2.1(2)	0.33(2)
0.1346	0.342(3)	3.08(18)	0.325(14)	0.374(4)	2.1(2)	0.30(2)
0.1350	0.319(4)	3.0(2)	0.314(16)	0.356(4)	2.0(3)	0.29(2)
0.1353	0.287(7)	2.2(3)	0.36(4)	0.326(8)	1.5(4)	0.33(5)

Table 18

Dipole fits of the neutron magnetic form factor.

$\kappa$	$A_m$	$aM_m$
$\beta = 6.0$		
0.1320	-1.68(9)	0.65(2)
0.1324	-1.78(9)	0.62(2)
0.1333	-1.71(14)	0.59(3)
0.1338	-1.6(2)	0.57(6)
0.1342	-1.6(3)	0.55(7)
$\beta = 6.2$		
0.1333	-1.90(8)	0.498(18)
0.1339	-1.78(9)	0.48(2)
0.1344	-1.90(15)	0.44(3)
0.1349	-1.70(16)	0.43(3)
$\beta = 6.4$		
0.1338	-2.05(8)	0.351(11)
0.1342	-2.06(16)	0.34(2)
0.1346	-2.01(14)	0.314(15)
0.1350	-1.84(16)	0.319(19)
0.1353	-1.5(2)	0.32(4)

## References

- [1] H.-Y. Gao, preprint nucl-ex/0301002.
- [2] M.K. Jones et al., Phys. Rev. Lett. 84 (2000) 1398.
- [3] O. Gayou et al., Phys. Rev. C64 (2001) 038202.
- [4] T. Draper, R.M. Woloshyn and K.F. Liu, Phys. Lett. B234 (1990) 121; D.B. Leinweber, R.M. Woloshyn and T. Draper, Phys. Rev. D43 (1991) 1659; W. Wilcox, T. Draper and K.F. Liu, Phys. Rev. D46 (1992) 1109.
- [5] V. Gadiyak, X. Ji and C. Jung, Phys. Rev. D65 (2002) 094510.
- [6] M. Lüscher, S. Sint, R. Sommer, P. Weisz and U. Wolff, Nucl. Phys. B491 (1997) 323.
- [7] D. Pleiter, Thesis, Freie Universität Berlin (2000).
- [8] C. Best, M. Göckeler, R. Horsley, E.-M. Ilgenfritz, H. Perlt, P. Rakow, A. Schäfer, G. Schierholz, A. Schiller and S. Schramm, Phys. Rev. D56 (1997) 2743.
- [9] M. Lüscher, S. Sint, R. Sommer and H. Wittig, Nucl. Phys. B491 (1997) 344.
- [10] T. Bakeyev, M. Göckeler, R. Horsley, D. Pleiter, P.E.L. Rakow, A. Schäfer, G. Schierholz and H. Stüben, preprint hep-lat/0209148.
- [11] M. Guagnelli and R. Sommer, Nucl. Phys. B (Proc. Suppl.) 63 (1998) 886; R. Sommer, private communication; S. Capitani, M. Göckeler, R. Horsley, H. Oelrich, H. Perlt, D. Pleiter, P.E.L. Rakow, G. Schierholz, A. Schiller and P. Stephenson, Nucl. Phys. B (Proc. Suppl.) 63 (1998) 233, 871.
- [12] S. Sint and P. Weisz, Nucl. Phys. B502 (1997) 251; S. Capitani, M. Göckeler, R. Horsley, H. Perlt, P.E.L. Rakow, G. Schierholz and A. Schiller, Nucl. Phys. B593 (2001) 183.
- [13] K.F. Liu, J. Phys. G 27 (2001) 511 and references therein.
- [14] S.J. Dong, K.F. Liu and A.G. Williams, Phys. Rev. D58 (1998) 074504; A.G. Williams, Nucl. Phys. B (Proc. Suppl.) 73 (1999) 306; N. Mathur and S.J. Dong, Nucl. Phys. B (Proc. Suppl.) 94 (2001) 311; W. Wilcox, Nucl. Phys. B (Proc. Suppl.) 94 (2001) 319.
- [15] R. Lewis, W. Wilcox and R.M. Woloshyn, Phys. Rev. D67 (2003) 013003.
- [16] S. Capitani, M. Göckeler, R. Horsley, B. Klaus, H. Oelrich, H. Perlt, D. Petters, D. Pleiter, P.E.L. Rakow, G. Schierholz, A. Schiller and P. Stephenson, Nucl. Phys. B (Proc. Suppl.) 73 (1999) 294.
- [17] M. Göckeler, R. Horsley, D. Pleiter, P.E.L. Rakow and G. Schierholz, in: *Lepton Scattering, Hadrons and QCD*, eds. W. Melnitchouk, A.W. Schreiber, A.W. Thomas and P.C. Tandy (World Scientific, Singapore, 2001), hep-ph/0108105.

- [18] T.R. Hemmert and W. Weise, Eur. Phys. J. A15 (2002) 487.
- [19] D.B. Leinweber, D.H. Lu and A.W. Thomas, Phys. Rev. D60 (1999) 034014.
- [20] D.B. Leinweber, A.W. Thomas and R.D. Young, Phys. Rev. Lett. 86 (2001) 5011.
- [21] E.J. Hackett-Jones, D.B. Leinweber and A.W. Thomas, Phys. Lett. B494 (2000) 89; G.V. Dunne, A.W. Thomas and S.V. Wright, Phys. Lett. B531 (2002) 77.
- [22] V. Bernard, H.W. Fearing, T.R. Hemmert and U.-G. Meißner, Nucl. Phys. A635 (1998) 121; 642 (1998) 563 (E).
- [23] P. Mergell, U.-G. Meißner and D. Drechsel, Nucl. Phys. A596 (1996) 367.
- [24] T.R. Hemmert, B.R. Holstein and J. Kambor, J. Phys. G24 (1998) 1831.
- [25] B. Kubis and U.-G. Meißner, Nucl. Phys. A679 (2001) 698.
- [26] N. Fettes, U.-G. Meißner, M. Mojzis and S. Steininger, Ann. Phys. 283 (2000) 273.
- [27] M.J. Savage, Nucl. Phys. A700 (2002) 359.
- [28] T.R. Hemmert, M. Procura and W. Weise, preprint hep-lat/0303002.
- [29] V. Bernard, N. Kaiser and U.-G. Meißner, Nucl. Phys. A611 (1996) 429.